Dynamic, intermediate, and static Jahn-Teller effect in the EPR spectra of ^2E orbital states

R. W. Reynolds
Advanced Technology Center, Incorporated, Dallas, Texas 75222

L. A. Boatner
Ecole Polytechnique Fédérale de Lausanne, Laboratoire de Physique Expérimentale, CH-1007 Lausanne, Switzerland
(Received 30 June 1975)

The intermediate Jahn-Teller effect which was observed for the specific systems CaO:Ag^{2+}, MgO:Ag^{2+}, CaO:Cu^{2+}, and CaF_2:Eu^{2+} has been successfully described previously by means of a vibronic coupling model in which the properties of the ground ^2E vibronic state were modified by random-strain coupling to an excited vibronic singlet level. The present work examines, in general, the question of how coupling via random strain between a ^2E vibronic level and an excited A_1 or A_2 vibronic singlet can result in the transition from the dynamic Jahn-Teller effect to the intermediate effect and finally to the limiting case of the static Jahn-Teller effect. The intermediate Jahn-Teller region is particularly important since it is possible in such cases to determine the ratio of the random-strain splitting $\bar{\delta}$ to the "tunneling" splitting 3Γ by EPR techniques. A similar determination using EPR cannot be made for systems characterized by either the limiting dynamic or static Jahn-Teller effect. The intermediate Jahn-Teller effect results in significant modifications to the EPR spectra which are characteristic of either the pure dynamic or pure static cases. These modifications include (i) changes in the angular variation, (ii) selective broadening of certain portions of the spectrum, and (iii) formation of complex line shapes for the orientation $\vec{H} \| \langle 111 \rangle$. A systematic calculation of the EPR line shapes and angular dependences has been performed for a range of values of $\bar{\delta}/3\Gamma$ which spans the intermediate Jahn-Teller region, and these features, which are tabulated graphically, illustrate the various types of intermediate Jahn-Teller spectra that may be observed experimentally. Additionally, a number of characteristic features of the isotropic spectrum resulting from thermal population of the first excited vibronic singlet level have been determined for the first time, and these results affect the validity of some of the criteria previously used to distinguish the possible origins of this spectrum.

I. INTRODUCTION

Ions with ^2E orbital ground states in cubic-symmetry hosts may exhibit any one of three types of Jahn-Teller (JT) effects in their low-temperature electron-paramagnetic-resonance (EPR) spectra. These effects have been designated as the static, dynamic, and intermediate JT effects. Of these types of JT effects, the static and dynamic effects are now comparatively well known owing to the relatively long period of time since their discovery and also to the relatively large number of systems whose low-temperature EPR spectra are characteristic of either a static or dynamic JT effect.[1-5] On the other hand, in the EPR spectra of ^2E orbital ground states, the identification of JT effects which are intermediate to the static and dynamic effects has only recently been accomplished.[7] In particular, these intermediate JT effects have been reported only for the EPR spectra of Cu^{2+}, Ag^{2+}, Ni^{2+}, and Ni^{3+} in MgO and for Cu^{2+} and Ag^{2+} in CaO (Refs. 6–11). An intermediate JT effect has also been reported[12] in the optically detected EPR spectrum of an excited state of Eu^{2+} in CaF_2.

The three types of JT effects exhibit the following basic distinguishing features: A static effect is characterized at low temperature by the presence of three magnetically inequivalent axially symmetric sites having principal symmetry axes along the cubic fourfold axes. The associated line shapes have the usual Gaussian or Lorentzian shapes frequently observed in electron-resonance experiments. The axially symmetric spectra will be motionally averaged as the temperature increases, and a resultant isotropic spectrum will be observed with $g = \frac{1}{3}(g_\parallel + 2g_\perp)$, where $g_\parallel$ and $g_\perp$ are appropriate to the low-temperature axially symmetric spectra. For the dynamic Jahn-Teller effect (in the absence of any hyperfine interaction), only one strain-broadened EPR line is present at low temperature. If the applied magnetic field is not parallel to one of the $\langle 111 \rangle$ axes, the greatest intensity of this strain-broadened line occurs near the two extremes rather than at the center, and the line has a shape similar to that of an EPR "powder" spectrum.[13] The values for the magnetic field positions of the extremes of this line display a cubic-symmetry variation which depends on the orientation of the applied magnetic field relative to the fourfold symmetry axes of the host crystal. At the magnetic field orientations corresponding to $\vec{H} \| \langle 100 \rangle$, the magnetic field extremes have their largest separation; at $\vec{H} \| \langle 111 \rangle$, this separation is essentially zero. The intensity of this anisotropic spectrum decreases with in-

creasing temperature until it is replaced by an isotropic spectrum which occurs at the magnetic field value coincident with that of the superimposed anisotropic extremes with $\vec{H} \| \langle 111 \rangle$. This isotropic resonance line can result from the averaging of part of the anisotropic line by rapid vibronic relaxation, by thermal population of the nearest excited vibronic singlet level, or by a combination of these effects. Some of the results of the present work provide new insight into the criteria previously used to distinguish between the two origins of the isotropic spectrum observed for systems characterized by the dynamic Jahn-Teller effect.

Intermediate JT effects manifest themselves by one or more of the following features: (i) a selective broadening and shifting of one extreme of an otherwise "pure" dynamic EPR spectrum; (ii) a departure of the angular variation of the spectrum from that associated with a pure dynamic or pure static JT effect; and (iii) the presence of unusually complex EPR line shapes for orientations corresponding to $\vec{H} \| \langle 111 \rangle$.[7]

Ham[1] and Chase[12] have developed a vibronic coupling model which describes the transition from dynamic to static JT effects for ^2E orbital states. We have found this model to be extremely successful in describing the details of the EPR spectra observed for Ag^{2+} in CaO and MgO (Ref. 7) and for Cu^{2+} in CaO (Ref. 6); the model also appears to be consistent with the MgO:Ni^{1+} and MgO:Ni^{3+} results (Ref. 8).

The elements of this theory are as follows: In the presence of vibronic coupling to a pair of localized vibrational modes which transform as the E irreducible representation of O_h, the ground state of the system composed of the ion and its nearest neighbors is a vibronic ^2E state. The first two excited states are A_1 and A_2 vibronic singlets whose order in energy will depend on the signs of the relevant Hamiltonian parameters. The energy separation of the ground state and the first excited singlet is known as the "tunneling" splitting 3Γ and is inversely dependent on the vibronic coupling strength. Purely dynamic Jahn-Teller effects will be observed in the EPR spectra when the tunneling splitting is large compared with the strength of other perturbations (e.g., random-strain and the Zeeman interaction) which could admix the ^2E and A_1 (or A_2) levels. In general, the random-strain interaction is expected to be greater than the Zeeman interaction. As the amount of admixture of either the A_1 or A_2 states with the ^2E state increases due to stronger vibronic coupling or greater random strain, the observed JT effects will become more characteristic of the static effect. If the average random-strain splitting of the ground ^2E vibronic state and the tunneling splitting are designated by $\bar{\delta}$ and 3Γ, respectively, then the ratio $\bar{\delta}/3\Gamma$ will determine whether dynamic, intermediate, or static JT effects are observed. Small values of $\bar{\delta}/3\Gamma$ ($\bar{\delta}/3\Gamma < 0.1$) correspond to a dynamic JT effect, while larger values ($\bar{\delta}/3\Gamma > 5$) result in a static effect. For values of $\bar{\delta}/3\Gamma$ between these limits, intermediate JT effects occur. The only EPR spectrum associated with a ^2E orbital state which is known to exhibit intermediate JT effects and which has not been completely described by this model is that of Cu^{2+} in MgO (Ref. 6). In this system, however, there are strong indications that appreciable random-strain coupling to both the A_1 and A_2 vibronic singlets is present. In the event of random-strain coupling to both vibronic singlets, a determination of the proper fit to an observed EPR spectrum becomes more difficult, and, to date, has not been attempted for the case of MgO:Cu^{2+}.

The present work has a threefold purpose. First, the general nature and characteristics of the dynamic, intermediate, and static Jahn-Teller effect for ^2E orbital states are examined in detail,[14] with particular emphasis being placed on the important intermediate Jahn-Teller region. In accomplishing this purpose, extensive calculations of the major spectral features (i.e., line shapes and angular variations) have been performed for a number of values of $\bar{\delta}/3\Gamma$ which were specifically selected to illustrate the transition from the dynamic to the static JT effect. These results have been summarized in a number of figures. Second, the analytical techniques which are required in order to make a determination of $\bar{\delta}/3\Gamma$ from the EPR results for a given specific system exhibiting the intermediate JT effect are presented. Finally, some characteristics associated with the isotropic spectrum resulting from thermal population of the first excited vibronic singlet are determined for the first time, and this information is discussed in terms of the various criteria which have been used in assigning the origin of this spectrum.

II. THEORY

A. General considerations

In the following discussion, frequent reference will be made to Fig. 1, which illustrates the roles of the various interactions affecting ^2E orbital electronic states of ions in cubic-symmetry hosts. As a frequently encountered example, let us consider a ^2D free-ion ground state representing, for example, the electronic ground state of an ion with a d^1 or d^9 configuration. In general, the static crystal-field interaction (i.e., ignoring vibrational effects) will produce the strongest

perturbation of the free-ion ground state. For cubic-symmetry crystal fields, the fivefold orbital degeneracy of the ^2D state will be removed, resulting in an orbital doublet and an orbital triplet designated respectively by ^2E and $^2T_2$ (Mulliken notation). For a d^1-configuration ion in eightfold cubic coordination or a d^9 configuration in sixfold cubic coordination, the ^2E state is lower in energy. In cubic symmetry the spin-orbit coupling does not split the ^2E state, but this interaction does produce small changes in the effective-Hamiltonian parameters for the ^2E state. Although Fig. 1 relates to d^1- or d^9-configuration ions in particular, the following discussion will be applicable in general to ^2E orbital states in cubic symmetry.

The next interaction to be considered is the vibronic coupling between the ^2E orbital state and the lattice vibrational modes. The simplest approach to treating the vibronic coupling in this case is to consider vibrational coupling of the ^2E orbital state to only two modes (i.e., Q_θ and Q_ϵ) which transform, respectively, as the θ and ϵ components of the E irreducible representation of O_h. These may be considered as the appropriately transforming normal modes of the cluster consisting of the ion and its nearest neighbors or, quoting Ham, "to represent in some average sense the various lattice distortion coordinates

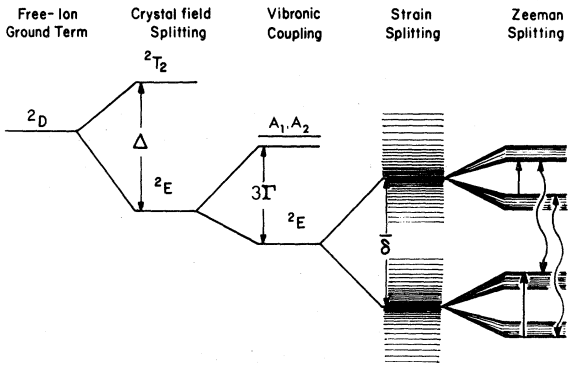

FIG. 1. Schematic representation of the effects of the cubic crystal field, vibronic coupling, strain splitting, and Zeeman interaction on a ^2D electronic state. Effects of the vibronic coupling, strain-splitting, and Zeeman interaction have been exaggerated relative to the crystal-field splitting Δ for the purposes of illustration. The ratio of the magnitude of the strain splitting $\bar{\delta}$ to the tunneling splitting 3Γ determines whether static, dynamic, or intermediate Jahn-Teller effects will be observed. Allowed ($\Delta M_S = \pm 1$, $\Delta M_I = 0$) EPR transitions are indicated by straight arrows at the right-hand side of the figure. Curved arrows correspond to vibronic relaxation effects which can produce an isotropic spectrum by averaging a portion of the strain-broadened resonance pattern (figure adapted from Ref. 4).

which belong to E and to which the Jahn-Teller coupling is most effective.[1]"

The Hamiltonian representing the vibronic coupling of the ^2E orbital state (composed of Ψ_θ and Ψ_ϵ electronic basis states) with the Q_θ and Q_ϵ modes then has the following form[1]:

$$\mathcal{H}_v = \{E_0 + (1/2\mu)[P_\theta^2 + P_\epsilon^2 + \mu^2\omega^2(Q_\theta^2 + Q_\epsilon^2)]\}\mathcal{T} + V(Q_\theta \mathcal{U}_\theta + Q_\epsilon \mathcal{U}_\epsilon) + \mathcal{H}_w, \quad (1)$$

where

$$\mathcal{H}_w = V_q[(Q_\epsilon^2 - Q_\theta^2)\mathcal{U}_\theta + 2Q_\epsilon Q_\theta \mathcal{U}_\epsilon] + V_c Q_\theta (Q_\theta^2 - 3Q_\epsilon^2)\mathcal{T}. \quad (2)$$

In the above equations E_0 is the electronic energy of the ^2E state in the absence of vibronic coupling, μ and ω are the reduced mass and the angular frequency of the mode, respectively, and P_θ and P_ϵ are the nuclear momentum operators conjugate to Q_θ and Q_ϵ, respectively. The parameters V, V_q and V_c are, respectively, the linear vibronic coupling, quadratic vibronic coupling, and anharmonic lattice force constants, while $\mathcal{T}$, $\mathcal{U}_\theta$, and $\mathcal{U}_\epsilon$ are the electronic orbital operators having the form

$$\mathcal{T} = \begin{bmatrix} +1 & 0 \\ 0 & +1 \end{bmatrix}; \quad \mathcal{U}_\theta = \begin{bmatrix} -1 & 0 \\ 0 & +1 \end{bmatrix}; \quad \mathcal{U}_\epsilon = \begin{bmatrix} 0 & +1 \\ +1 & 0 \end{bmatrix} \quad (3)$$

with respect to the Ψ_θ and Ψ_ϵ electronic basis states. The nonlinear coupling or "warping" terms are designated by $\mathcal{H}_w$.

Solutions to Eq. (1) cannot be obtained analytically. However, as pointed out by Ham, the Hamiltonian maintains cubic symmetry under simultaneous transformations of the electronic and vibrational operators, and the resulting vibronic states must therefore transform as the same irreducible representations of O_h as those of the electronic states in the absence of coupling.[1] It has been shown[15] that for all values of V, the vibronic ground state resulting from solutions to Eq. (1) is a vibronic ^2E level. In the absence of warping terms, the first excited level is a doublet composed of accidentally degenerate A_1 and A_2 singlets. Warping terms remove this degeneracy; which singlet lies at lower energy depends upon the signs and magnitudes of the parameters V, V_q, and V_c in Eqs. (1) and (2). The energy separation between the ground ^2E and the first excited singlet is the tunneling splitting 3Γ, which depends inversely on the strength of the vibronic coupling.

Random strain with tetragonal symmetry will lift the twofold degeneracy of the ^2E vibronic state, and the large number of different strain-split levels shown in Fig. 1 represents the effects of the distribution of strain from site to site in the crystal. The remaining Kramers degeneracy of each

strain-split state is then removed by the Zeeman interaction when an external magnetic field is applied (as it is in the course of a conventional magnetic-resonance experiment). Two of the allowed ($\Delta M_S = \pm 1$) EPR transitions are indicated by the straight arrows at the right-hand side of Fig. 1.

The characteristics of the EPR spectrum resulting from the interactions discussed above are strongly dependent on the relative magnitudes of splittings due to tunneling, random-strain, and the Zeeman interaction. If the tunneling splitting is large compared with the random-strain and Zeeman splittings, then the low-temperature EPR spectrum is determined only by the random-strain and Zeeman splitting of the ^2E vibronic state. However, if the vibronic coupling terms are large enough that 3Γ is comparable in magnitude to the random-strain and Zeeman interactions, the resulting ground vibronic state contains an admixture of the ^2E state with either one or both vibronic singlets, depending on the magnitude of the warping terms. The EPR spectrum which corresponds to this admixture of states will in general have greatly different properties from that corresponding to a pure ^2E vibronic state.

In the present work we will consider coupling to only one of the two excited singlet levels in calculating the eigenvectors of the random-strain interaction within the three-state manifold. This simplification is warranted since there is presently only one reported case[6] in which there is evidence for coupling to both excited singlets (i.e., the case of Cu^{2+} in MgO).

Ham[1] has given a generalized matrix form for those interactions which may perturb the manifold containing the ^2E state and the next excited singlet level. For A_1 lower, this matrix has the following form with respect to the basis states Ψ_{A_1}, $\Psi_{g\theta}$, and $\Psi_{g\epsilon}$:

$$\begin{array}{c} \\ \Psi_{A_1}: \\ \Psi_{g\theta}: \\ \Psi_{g\epsilon}: \end{array} \begin{array}{c} \begin{array}{ccc} \Psi_{A_1} & \Psi_{g\theta} & \Psi_{g\epsilon} \end{array} \\ \begin{pmatrix} 3\Gamma + G_1 & rG_\theta & rG_\epsilon \\ rG_\theta & G_1 - qG_\theta & qG_\epsilon \\ rG_\epsilon & qG_\epsilon & G_1 + qG_\theta \end{pmatrix} \end{array} , \tag{4}$$

where $\Psi_{g\theta}$ and $\Psi_{g\epsilon}$ are the two components of the ^2E vibronic state which transform as the θ and ϵ components of the E representation.

The corresponding matrix[1] for A_2 lower is

$$\begin{array}{c} \\ \Psi_{A_2}: \\ \Psi_{g\theta}: \\ \Psi_{g\epsilon}: \end{array} \begin{array}{c} \begin{array}{ccc} \Psi_{A_2} & \Psi_{g\theta} & \Psi_{g\epsilon} \end{array} \\ \begin{pmatrix} 3\Gamma + G_1 & rG_\epsilon & -rG_\theta \\ rG_\epsilon & G_1 - qG_\theta & qG_\epsilon \\ -rG_\theta & qG_\epsilon & G_1 + qG_\theta \end{pmatrix} \end{array} . \tag{5}$$

Operators transforming as the A_2 irreducible representation of O_h have been omitted from these matrices as we will not be concerned here with any interactions transforming as A_2.

In the above matrices q and r are the reduction factors of Ham which are defined by the relations

$$q = -\langle \Psi_{g\theta} | \mathfrak{U}_\theta | \Psi_{g\theta} \rangle = \langle \Psi_{g\epsilon} | \mathfrak{U}_\theta | \Psi_{g\epsilon} \rangle = \langle \Psi_{g\epsilon} | \mathfrak{U}_\epsilon | \Psi_{g\theta} \rangle \tag{6}$$

and

$$r = \langle \Psi_{A_1} | \mathfrak{U}_\theta | \Psi_{g\theta} \rangle = \langle \Psi_{A_1} | \mathfrak{U}_\epsilon | \Psi_{g\epsilon} \rangle \tag{7}$$

or

$$r = \langle \Psi_{A_2} | \mathfrak{U}_\epsilon | \Psi_{g\theta} \rangle = -\langle \Psi_{A_2} | \mathfrak{U}_\theta | \Psi_{g\epsilon} \rangle . \tag{8}$$

The reduction factors shown above express the changes in the expectation value of the orbital operators $\mathfrak{U}_\theta$ and $\mathfrak{U}_\epsilon$ that result from the vibronic coupling. For zero vibronic coupling $q = 1$, for strong linear vibronic coupling $q = -r = \frac{1}{2}$, and for strong vibronic coupling with appreciable warping (i.e., so that the vibrational parts of the strong-JT-coupled wave functions do not overlap), the relation given by $q = -r/\sqrt{2} = \frac{1}{2}$ is valid.[1]

The operators G_1, G_θ, and G_ϵ are functions of the relevant perturbations which transform, respectively, as A_1, E_θ, and E_ϵ. These operators are independent of Q_θ and Q_ϵ. For random strain the operators have the form

$$G_\theta = V_2 e_\theta \quad \text{and} \quad G_\epsilon = V_2 e_\epsilon , \tag{9}$$

where V_2 is the strain coupling parameter and e_θ and e_ϵ are the components of the random strain which transform, respectively, as the E_θ and E_ϵ components of E. In terms of the diagonal components of the strain tensor, the e_θ and e_ϵ components of the strain are defined as follows:

$$\begin{aligned} e_\theta &= \tfrac{1}{2}(2e_{zz} - e_{xx} - e_{yy}), \\ e_\epsilon &= \tfrac{1}{2}\sqrt{3}\,(e_{xx} - e_{yy}) . \end{aligned} \tag{10}$$

For the Zeeman and hyperfine interactions, respectively, the operators have the form

$$\begin{aligned} &G_1 = g_1 \mu_B \vec{H} \cdot \vec{S}, \quad G_\theta = \tfrac{1}{2} g_2 \mu_B (3H_z S_z - \vec{H} \cdot \vec{S}), \\ &G_\epsilon = \tfrac{1}{2}\sqrt{3}\, g_2 \mu_B (H_x S_x - H_y S_y) \end{aligned} \tag{11}$$

and

$$\begin{aligned} &G_1 = A_1 \vec{I} \cdot \vec{S}, \quad G_\theta = \tfrac{1}{2} A_2 (3I_z S_z - \vec{I} \cdot \vec{S}), \\ &G_\epsilon = \tfrac{1}{2}\sqrt{3}\, A_2 (I_x S_x - I_y S_y), \end{aligned} \tag{12}$$

where $\vec{S}$ and $\vec{I}$ are, respectively, the electronic and nuclear-spin operators and μ_B is the Bohr magneton.

Assuming that the cubic crystal-field interaction is large with respect to the spin-orbit coupling, first-order expressions for g_1, g_2, A_1, and A_2

may be obtained using crystal-field theory. These expressions are given by the following equations:

$$g_1 = 2.0023 - 4\lambda/\Delta, \tag{13}$$

$$g_2 = -4\lambda/\Delta = g_1 - 2.0023, \tag{14}$$

$$A_1 = (-2\mu_B\mu\langle r^{-3}\rangle/I)(\kappa + 4\lambda/\Delta), \tag{15}$$

$$A_2 = (-2\mu_B\mu\langle r^{-3}\rangle/I)(\tfrac{4}{7} + 34\lambda/7\Delta), \tag{16}$$

where Δ, λ, μ, $\langle r^{-3}\rangle$, and κ are, respectively, the cubic crystal-field splitting $10Dq$, the spin-orbit coupling parameter, the nuclear magnetic dipole moment, the one-electron expectation value of r^{-3}, and the Fermi contact parameter. The effects of covalency can result in modifications to these equations, and, accordingly, their implications should be viewed with an appropriate degree of caution.

The relative magnitudes of the tunneling, random-strain, and Zeeman interactions which enter into the matrices in Eqs. (4) and (5) will determine whether dynamic , static, or intermediate JT effects are observed in the EPR spectra associated with the eigenstates of these matrices. In the Secs. II B–II D, the origins and characteristics of the three types of JT effects will be described as they result from the eigenstates of Eqs. (4) and (5).

B. Dynamic Jahn-Teller effects

If 3Γ is large compared with the random-strain and Zeeman interactions, then the admixture of the first excited singlet into the ground state is negligible. The EPR spectrum at low temperature is then determined only by the properties of the ^2E vibronic state and the strain interaction. This condition is known as the dynamic limit, and the EPR spectrum is said to exhibit a low-temperature dynamic JT effect. If the random-strain interaction Eq. (9) is substituted into Eqs. (4) and (5) and 3Γ is assumed to be large compared to the random strain, then the resulting eigenstates within the ^2E vibronic state are

$$\Psi_+ = \sin(\tfrac{1}{2}\phi)\Psi_{g\theta} + \cos(\tfrac{1}{2}\phi)\Psi_{g\epsilon}, \tag{17}$$

$$\Psi_- = \cos(\tfrac{1}{2}\phi)\Psi_{g\theta} - \sin(\tfrac{1}{2}\phi)\Psi_{g\epsilon}, \tag{18}$$

where $\tan\phi = e_\epsilon/e_\theta$ gives the distribution of random strain between the θ and ϵ components. The states Ψ_+ and Ψ_- are separated in energy by a strain splitting δ which is given by the expression

$$\delta = 2q|V_2|(e_\theta^2 + e_\epsilon^2)^{1/2}. \tag{19}$$

In the presence of Zeeman and hyperfine interactions which are small compared to the random-strain splitting, the EPR spectrum is determined by the expectation value of the operators in Eqs. (9)–(12) within the Ψ_+ and Ψ_- eigenstates. If in addition qg_2/g_1, qA_2/A_1, and $A_1/g_1\mu_B H$ are assumed small, the frequencies of the allowed ($\Delta M_S = \pm 1$, $\Delta M_I = 0$) EPR transitions within each of two Kramers doublets are given to second order by the expression[5]

$$h\nu_\pm = \left(g_1 \pm \tfrac{1}{2}qg_2 f_1 + \frac{(qg_2)^2}{g_1} f_3\right)\mu_B H + \left(A_1 \pm \tfrac{1}{2}qA_2 f_1 + \frac{(qA_2)^2}{A_1} f_3 + 2\frac{qg_2}{g_1} qA_2 f_3\right) M_I + \left(\frac{(A_1 \mp \frac{1}{4}qA_2 f_1)^2}{2g_1\mu_B H} + \frac{(qA_2)^2}{g_1\mu_B H} f_4\right)[I(I+1) - M_I^2] + \frac{(qA_2)^2}{g_1\mu_B H} f_3 M_I^2, \tag{20}$$

where

$$f_1 = (3n^2 - 1)\cos\phi + \sqrt{3}(l^2 - m^2)\sin\phi,$$

$$f_3 = \tfrac{1}{8}\{2 - [(3n^2 - 1)\cos\phi + \sqrt{3}(l^2 - m^2)\sin\phi]^2 - [-(3n^2 - 1)\cos 2\phi + \sqrt{3}(l^2 - m^2)\sin 2\phi]\},$$

$$f_4 = \tfrac{1}{32}\{4 + [(3n^2 - 1)\cos\phi + \sqrt{3}(l^2 - m^2)\sin\phi]^2 + 4[-(3n^2 - 1)\cos 2\phi + \sqrt{3}(l^2 - m^2)\sin 2\phi]\}.$$

In Eq. (20) above, M_I represents the nuclear spin projection quantum number. The ($\pm$) subscript differentiates the solutions for the two Kramers doublets $\Psi_\pm$. In these equations, l, m, and n are the direction cosines of the applied magnetic field relative to the cubic fourfold axes. The distribution in the components of internal strain from site to site in the crystal is expected to be random so that all values of ϕ in the region $0 \leq \phi \leq 2\pi$ will be equally likely. As a result, the EPR spectrum from a macroscopic sample has the EPR transitions distributed in a manner consistent with Eq. (20), and the corresponding EPR spectrum is found to have a shape similar to an EPR powder spectrum.

In order to provide a proper background for subsequent discussions, it is desirable to discuss the nature of the peaks in EPR spectra when $\vec{H}$ is oriented in a $\{110\}$ plane. For either Kramers doublet resulting from the strain splitting and for H in a $\{110\}$ plane, the two peaks of the strain-broadened EPR line are associated with those sites

having $\phi = 0$ or $\phi = \pi$ (i.e., with those sites having $e_\epsilon = 0$). Ions at sites with $\phi = 0$ are described by the wave functions $\Psi_+ = \Psi_{g\epsilon}$ and $\Psi_- = \Psi_{g\theta}$, with Ψ_- at lower energy (assuming V_2 is positive). For ions at sites with $\phi = \pi$, the corresponding wave functions are $\Psi_+ = \Psi_{g\theta}$ and $\Psi_- = -\Psi_{g\epsilon}$, with Ψ_- at lower energy. If qg_2 is positive (e.g., d^9-configuration ions), then [from Eq. (20)] for both Kramers doublets $\Psi_{g\theta}$ is associated with the high-field peak of the strain-broadened line for magnetic field orientations with $1 \geq n > 1/\sqrt{3}$ and with the low-field peak for $1/\sqrt{3} > n \geq 0$. Ions described by $\Psi_{g\epsilon}$ are associated with the opposite peak of the spectrum at each magnetic field orientation. If qg_2 is negative (e.g., d^1-configuration ions), the above association of $\Psi_{g\theta}$ and $\Psi_{g\epsilon}$ with particular peaks of the spectrum is reversed at any given magnetic field orientation. The features described above comprise the "pure dynamic" case, which corresponds to a ^2E state in cubic symmetry with the A_1 and A_2 vibronic singlets separated from this state by an amount such that the EPR spectra do not exhibit the effects of coupling between the doublet and singlet levels.

C. Intermediate Jahn-Teller effects

As the ratio $\bar{\delta}/3\Gamma$ is increased from its value appropriate to the pure dynamic case, interesting changes in the EPR spectrum are produced by the effects of admixture of the first excited vibronic singlet level with the ground ^2E vibronic state.[12] This admixture occurs through the combined effects of random-strain and Zeeman interactions. As an example of these changes, let us assume the following conditions: (i) The A_1 singlet is appreciably lower in energy than the A_2 singlet; (ii) the splitting (3Γ) between the A_1 and ^2E states is comparable in magnitude to the random-strain splitting of the ^2E state so that the A_1 and ^2E have a small, but appreciable, admixture due to the random strain; (iii) the Zeeman interaction is much smaller than the random-strain interaction so that the admixture due to the magnetic field is negligible; and (iv) the magnetic field is oriented in a $\{110\}$ plane. If 3Γ is still sufficiently large so that second-order perturbation theory can be employed for the random-strain interaction, then from Eqs. (4), (5), (17), and (18), the perturbed ^2E wave functions $\Psi'_{g\theta}$ and $\Psi'_{g\epsilon}$ are given by

$$\Psi'_{g\theta} \simeq \Psi_{g\theta} - (rV_2 e_\theta/3\Gamma)\Psi_{A1}\,, \qquad \Psi'_{g\epsilon} \simeq \Psi_{g\epsilon} \tag{21}$$

for sites with $\phi = 0$ or $\phi = \pi$. For $\phi = 0$ or $\phi = \pi$, only the $\Psi_{g\theta}$ state is perturbed by random-strain coupling (to second order), and therefore only the EPR peak associated with $\Psi_{g\theta}$ for these sites will be affected. The expectation values for the Zeeman interaction H_z within the upper and lower Kramers doublets (Ψ'_+ and Ψ'_-) resulting from the perturbed ^2E are given by

$$\langle\Psi'_+|H_z|\Psi'_+\rangle = \langle\Psi'_{g\epsilon}|H_z|\Psi'_{g\epsilon}\rangle \simeq \langle\Psi_{g\epsilon}|H_z|\Psi_{g\epsilon}\rangle = G_1 + qG_\theta\,, \tag{22}$$

$$\langle\Psi'_-|H_z|\Psi'_-\rangle = \langle\Psi'_{g\theta}|H_z|\Psi'_{g\theta}\rangle \simeq \langle\Psi_{g\theta}|H_z|\Psi_{g\theta}\rangle - (2rV_2e_\theta/3\Gamma)\langle\Psi_{g\theta}|H_z|\Psi_{A1}\rangle \simeq G_1 - (q + 2r^2V_2e_\theta/3\Gamma)G_\theta \tag{23}$$

for sites with $\phi = 0$, while for sites with $\phi = \pi$, these relations are

$$\langle\Psi'_+|H_z|\Psi'_+\rangle \simeq \langle\Psi_{g\theta}|H_z|\Psi_{g\theta}\rangle - (2rV_2e_\theta/3\Gamma)\langle\Psi_{g\theta}|H_z|\Psi_{A1}\rangle \simeq G_1 - (q + 2r^2V_2e_\theta/3\Gamma)G_\theta\,, \tag{24}$$

$$\langle\Psi'_-|H_z|\Psi'_-\rangle \simeq \langle\Psi_{g\epsilon}|H_z|\Psi_{g\epsilon}\rangle = G_1 + qG_\theta\,. \tag{25}$$

Here G_1 and G_θ represent the Zeeman interaction [Eq. (11)]. According to Eqs. (22)–(25), for each Kramers doublet only one of the two peaks of the spectrum is affected by random-strain coupling to the excited singlet, and that peak is the one which is associated with $\Psi_{g\theta}$. The effect of this coupling is to change the coefficient of the anisotropic part of the Zeeman interaction (G_θ) for sites described by $\Psi_{g\theta}$ states. For the ground Kramers doublet, the anisotropy of the $\Psi_{g\theta}$ peak is increased for increasing $|e_\theta|/3\Gamma$ since (in Eq. 23) q and $2r^2V_2e_\theta/3\Gamma$ are positive. For the excited doublet, this anisotropy decreases for increasing $|e_\theta|/3\Gamma$ since q and $2r^2V_2e_\theta/3\Gamma$ are of opposite sign in Eq. (25) (i.e., e_θ is negative for $\phi = \pi$). For qg_2 positive and H in a $\{110\}$ plane with $1 \geq n > 1/\sqrt{3}$, it is the high-field peak of both doublets that is associated with $\Psi_{g\theta}$. Therefore, for the above conditions on qg_2 and n, it is the high-field peak of both doublets that is broadened and shifted by random-strain coupling, with the high-field peak of the lower doublet shifted to higher field and the high-field peak of the upper doublet shifted to lower field.

If the lower singlet is the A_2 level, then by the same arguments as those leading to Eqs. (22)–(25) it is the $\Psi_{g\epsilon}$ peak that is affected by the random-strain coupling. For A_2 lower, the shift in the magnetic field position of the $\Psi_{g\theta}$ peak is in the direction of increasing anisotropy for the ground doublet and decreasing anisotropy for the excited doublet (just as in the case for A_1 lower). The conclusions from the proceeding arguments are summarized in Table I.

Although we are dealing with a continuous range of effects as the ratio $\bar{\delta}/3\Gamma$ varies in the intermediate JT region, we have found it very useful to introduce two new general (and slightly overlapping) classifications in describing the observed EPR

spectra. These classifications are, first, "quasidynamic," which describes those EPR spectra whose angular variations are a modified form of the variation described by Eq. (20) with one side or the other broadened and shifted in the manner discussed previously. Accordingly, the three distinct tetragonal spectra characteristic of the static Jahn-Teller effect are not observed. The quasidynamic classification is appropriate to the general region of $\bar{\delta}/3\Gamma$ values given by $0.1 < \bar{\delta}/3\Gamma < 0.8$. The second classification, termed "quasistatic," applies to those systems where three tetragonal-symmetry EPR spectra are observed, but where distortions in the EPR line shapes are present. The quasistatic classification applies to the general region of $\bar{\delta}/3\Gamma$ values given by $0.3 < \bar{\delta}/3\Gamma < 5.0$.

D. Static Jahn-Teller effects

The final case to be considered results when the random-strain splitting is much larger than the tunneling splitting. This condition is known as the static limit, and the EPR spectrum is said to exhibit a "pure static" JT effect if three distinct tetragonal symmetry spectra are observed and if $\bar{\delta}/3\Gamma$ is sufficiently large to permit the observation of symmetric EPR line shapes (typically $\bar{\delta}/3\Gamma > 5.0$). In the static limit, the interactions which affect the ^2E and $A_1(A_2)$ manifold can be more clearly expressed relative to a new set of vibronic basis states. These states, Ψ_1, Ψ_2, and Ψ_3, are defined by the expressions

$$\Psi_{A1} = (1/\sqrt{3})(\Psi_1 + \Psi_2 + \Psi_3)\,,$$
$$\Psi_{g\theta} = (1/\sqrt{6})(2\Psi_1 - \Psi_2 - \Psi_3), \quad \Psi_{g\epsilon} = (1/\sqrt{2})(\Psi_2 - \Psi_3) \tag{26}$$

for A_1 lower, or by the expressions

TABLE I. Effect of random-strain coupling to an excited vibronic singlet on the EPR spectrum of a ^2E state; for $\vec{H}$ in a $\{110\}$ plane with $1 \geq n > 1/\sqrt{3}$. Relations are reversed for $1/\sqrt{3} > n \geq 0$.

Sign of qg_2	Coupled singlet	Shifted peak Position	Direction
	Ground Kramers doublet		
+	A_1	high field	to high field
+	A_2	low field	to low field
−	A_1	low field	to low field
−	A_2	high field	to high field
	First excited Kramers doublet		
+	A_1	high field	to low field
+	A_2	low field	to high field
−	A_1	low field	to high field
−	A_2	high field	to low field

$$\Psi_{A2} = (1/\sqrt{3})(\Psi_1 + \Psi_2 + \Psi_3), \quad \Psi_{g\theta} = (1/\sqrt{2})(\Psi_3 - \Psi_2)\,, \tag{27}$$
$$\Psi_{g\epsilon} = (1/\sqrt{6})(2\Psi_1 - \Psi_2 - \Psi_3)$$

for A_2 lower.

Relative to the Ψ_1, Ψ_2, and Ψ_3 basis, the generalized matrix elements in Eqs. (4) and (5) have the form given by the following relations:

$$\mathcal{H}_{11} = \Gamma + G_1 \mp \tfrac{2}{3}(q - \sqrt{2}\,r)G_\theta\,,$$
$$\mathcal{H}_{22} = \Gamma + G_1 \mp \tfrac{1}{3}(q - \sqrt{2}\,r)(-G_\theta + \sqrt{3}G_\epsilon)\,,$$
$$\mathcal{H}_{33} = \Gamma + G_1 \mp \tfrac{1}{3}(q - \sqrt{2}\,r)(-G_\theta - \sqrt{3}G_\epsilon)\,, \tag{28}$$
$$\mathcal{H}_{12} = \mathcal{H}_{21} = \Gamma \pm \tfrac{1}{6}\sqrt{2}(\sqrt{2}\,q + r)(G_\theta + \sqrt{3}\,G_\epsilon)\,,$$
$$\mathcal{H}_{13} = \mathcal{H}_{31} = \Gamma \pm \tfrac{1}{6}\sqrt{2}(\sqrt{2}\,q + r)(G_\theta - \sqrt{3}\,G_\epsilon)\,,$$
$$\mathcal{H}_{23} = \mathcal{H}_{32} = \Gamma \pm \tfrac{1}{3}\sqrt{2}(\sqrt{2}\,q + r)G_\theta\,,$$

where $\mathcal{H}_{ij} = \langle \Psi_i | \mathcal{H} | \Psi_j \rangle$, with $i,j = 1,2,3$. The upper signs are required for A_1 lower and the lower signs for A_2 lower.

For strong vibronic coupling and large warping effects, it can be shown that each of the Ψ_1, Ψ_2, and Ψ_3 states corresponds to a vibronic state whose vibrational part represents a distortion along one of the cubic fourfold axes. Under these conditions, the relation $r = -\sqrt{2}q$ can be shown to be valid, so that the diagonal matrix elements in Eq. (28) become

$$\mathcal{H}_{11} = \Gamma + G_1 \mp 2qG_\theta, \quad \mathcal{H}_{22} = \Gamma + G_1 \mp q(-G_\theta + \sqrt{3}\,G_\epsilon)\,, \tag{29}$$
$$\mathcal{H}_{33} = \Gamma + G_1 \mp q(-G_\theta - \sqrt{3}\,G_\epsilon)\,,$$

and all off-diagonal elements are equal to Γ. In general, one can assume that the random-strain and tunneling interactions are much larger than the Zeeman and hyperfine interactions. If this condition holds, then in order to calculate the EPR spectrum for the $^2E - A$ manifold, it is first necessary to diagonalize the matrix associated with Eqs. (29) for various values of the random strain. After the eigenstates of Eqs. (29) are determined, it is sufficient to compute the expectation values of the Zeeman and hyperfine interactions within these eigenstates by first-order perturbation theory. (It should be noted that for EPR experiments performed at high frequencies the Zeeman interaction may have to be included in the initial diagonalization. A procedure of this type can, however, permit the independent determination of $\bar{\delta}$ and 3Γ. See Refs. 6 and 10.)

If Eq. (9) is substituted into Eq. (29), the resulting matrix of random strain and tunneling has the form given by

$$\begin{array}{c} \\ \Psi_1: \\ \Psi_2: \\ \Psi_3: \end{array} \begin{array}{c} \begin{array}{ccc} \Psi_1 & \Psi_2 & \Psi_3 \end{array} \\ \begin{pmatrix} \Gamma \mp \delta\cos\phi/2q & \Gamma & \Gamma \\ \Gamma & \Gamma \pm \delta(\cos\phi - \sqrt{3}\sin\phi)/2q & \Gamma \\ \Gamma & \Gamma & \Gamma \pm \delta(\cos\phi + \sqrt{3}\sin\phi)/2q \end{pmatrix} \end{array}, \tag{30}$$

where $\delta = 2q\,|V_2|\,(e_\theta^2 + e_\epsilon^2)^{1/2}$ is the strain splitting appropriate to the isolated ^2E state,

$$e_\epsilon = (\delta\sin\phi)/2q\,|V_2|\,,$$
$$e_\theta = (\delta\cos\phi)/2q\,|V_2|\,, \tag{31}$$

and where ϕ determines the distribution of strain between θ and ϵ components. Again, the upper and lower signs correspond, respectively, to either the A_1 or A_2 singlet lower in energy. If $\delta \gg 3\Gamma$, then the eigenvectors of Eq. (30) are Ψ_1, Ψ_2, and Ψ_3. The expectation value of the Zeeman and hyperfine interactions within each of these Kramers doublets is given by the equations

$$\begin{aligned} \mathcal{H}_{11} &= \Gamma + g_\parallel \mu_B H_z S_z + g_\perp \mu_B (H_x S_x + H_y S_y) \\ &\quad + A_\parallel S_z I_z + A_\perp (S_x I_x + S_y I_y)\,, \\ \mathcal{H}_{22} &= \Gamma + g_\parallel \mu_B H_x S_x + g_\perp \mu_B (H_z S_z + H_y S_y) \\ &\quad + A_\parallel S_x I_x + A_\perp (S_z I_z + S_y I_y)\,, \\ \mathcal{H}_{33} &= \Gamma + g_\parallel \mu_B H_y S_y + g_\perp \mu_B (H_x S_x + H_z S_z) \\ &\quad + A_\parallel S_y I_y + A_\perp (S_x I_x + S_z I_z)\,, \end{aligned} \tag{32}$$

where $S = \frac{1}{2}$, $g_\parallel = g_1 \mp 2qg_2$, $g_\perp = g_1 \pm qg_2$, $A_\parallel = A_1 \mp 2qA_2$, and $A_\perp = A_1 \pm qA_2$. Again, the upper (lower) sign corresponds to the A_1 (A_2) state being lowest. (It should be noted that the same A_1, A_2 notation is conventionally used to label both the vibronic excited states and the hyperfine parameters.) It is obvious that Eqs. (32) contain the spin-Hamiltonian relations for axially symmetric sites having unique principal axes along the z, x, and y axes, respectively. Thus in the limit $\delta \gg 3\Gamma$, the static JT effect described by Eqs. (32) is observed. Also, when $\delta \gg 3\Gamma$, each of the three $\Psi_i (i = 1, 2, 3)$ becomes the ground state as ϕ is varied between the limits $0 < \phi < 2\pi$. Since within a given crystal all values of ϕ in the range $0 < \theta < 2\pi$ are expected to be present, only the ground Kramers doublet need be populated in order to observe the EPR spectrum due to each of the three axial sites described by Eqs. (32).

E. Calculations of EPR spectra in intermediate and limiting cases

For values of $\bar{\delta}/3\Gamma$ which are intermediate to the static or dynamic limits, it is most convenient to diagonalize Eq. (30) in order to determine the eigenvectors. Once the eigenvectors

$$\Phi_i = \sum_{j=1}^{3} C_{ij}\Psi_j$$

are determined, the expectation values of the Zeeman and hyperfine interactions $\langle \Phi_i | \mathcal{H}_z | \Phi_i \rangle$ are easily calculated, since $\langle \Psi_j | \mathcal{H}_z | \Psi_k \rangle$ is diagonal when $r = -\sqrt{2}q$. In the present investigation, this general procedure was used to calculate the EPR spectra associated with ions described by varying magnitudes of $\bar{\delta}/3\Gamma$. The details of this procedure are described below.

The primary emphasis in this work is placed on the changes in EPR line shapes as a function of varying $\bar{\delta}/3\Gamma$ ratios; in particular, it was judged most important to illustrate the line shape changes as $\bar{\delta}/3\Gamma$ is varied in the range $0.1 \leq \bar{\delta}/3\Gamma \leq 5.0$, where the transition from dynamic to static JT effects is observed. In order to reduce the variable parameters in this calculation to a manageable number, it was necessary to fix the values of r and q. The assumption of fixed values for r and q is to some degree an approximation since r, q, and 3Γ are all dependent on the strength and type of JT interaction (i.e., the ratio of linear coupling to warping terms and the ratio of $E_{JT} = V^2/2\mu\omega^2$ to $\hbar\omega$). For strong JT coupling ($E_{JT} \gg \hbar\omega$), the relations

$$q \simeq \tfrac{1}{2}[1 + (\hbar\omega/4E_{JT})^2] \tag{33}$$

and

$$r = -q(1 - 3\epsilon)\sqrt{2} \tag{34}$$

have been shown[16] to be valid, where ϵ is a parameter which depends on the ratio of warping to linear JT coupling terms. For small warping, $\epsilon \simeq 0.1$, so that $r \simeq -q$. As the warping increases relative to the linear JT coupling, ϵ decreases rapidly so that $r = -\sqrt{2}q$ for large warping and strong JT coupling.[16] Unless otherwise stated, the values $q = \frac{1}{2}$ and $r = -\sqrt{2}q$ were used in the calculations presented here. These values should be fairly accurate throughout the transition region from static to dynamic JT effects.

Although the magnitude of the random strain present within a crystal is expected to have a spatial distribution, little is known about the details of this distribution. Accordingly, some assumptions must be made in order to calculate the EPR spectrum for the ensemble of sites. A Gaussian

distribution about a mean strain splitting $\bar{\delta}$ was used in the present calculations, with the probability of any site having a random-strain splitting δ given by $P(\delta)$ where

$$P(\delta) \propto \exp[-(\delta-\bar{\delta})^2/2\sigma^2]. \quad (35)$$

A distribution about a nonzero mean splitting was assumed in order to achieve consistency with the previous assumption that the Zeeman interaction is small relative to the random-strain splitting.

In order to calculate a particular EPR spectrum, values of g_1, qg_2, $\bar{\delta}$ (standard deviation of the strain splitting), 3Γ, kT, l, m, and n were chosen. (Values for the hyperfine parameters and the other effective-Hamiltonian parameters determined by fitting the angular variation were used in calculating line shapes for comparison with experimental data.) A set of $\delta/3\Gamma$ values was then chosen with these values uniformly distributed about $\bar{\delta}/3\Gamma$. For each $\delta/3\Gamma$ value, a fixed number ($\approx$200) of ϕ values uniformly distributed over a range $0 \leq \phi \leq 2\pi$ was chosen, and the matrix in Eq. (30) was numerically diagonalized for each value of ϕ and $\delta/3\Gamma$. For each diagonalization, the Zeeman (and hyperfine) splitting of each Kramers doublet was calculated, and the corresponding resonance magnetic field values were computed, assuming the usual allowed ($\Delta M_S = \pm 1$, $\Delta M_I = 0$) EPR transitions. A Gaussian line shape with arbitrary width was associated with each EPR transition to account for dipolar line broadening. The EPR spectrum for the ensemble of sites was then determined by weighting the EPR intensity at each resonance magnetic field value by both the Boltzmann factor appropriate to the assumed temperature and by the probability distribution for δ which is given in Eq. (35). The intensity was then summed over all δ and ϕ values. For a given value of $\bar{\delta}/3\Gamma$, the EPR line shape could be varied by changing either the width of the component EPR lines or the width of $P(\delta)$. In the work presented here, σ was set equal to $\bar{\delta}$ and the width of the component EPR lines was adjusted to give a reasonably smooth EPR line shape for the composite crystal.

The maximum computed EPR absorption intensity over the range of resonance magnetic values depends strongly on the assumed $\bar{\delta}/3\Gamma$ value. In particular, as $\bar{\delta}/3\Gamma$ is increased in going toward the static limit, the EPR spectrum varies from a relatively wide absorption band to three individual sharp EPR lines. Consequently, normalization of the integrated EPR intensity for systems with different $\bar{\delta}/3\Gamma$ values would obscure the line-shape changes that occur in systems with lower maximum EPR absorption intensity. For this reason, such a normalization was not performed for the computed EPR spectra presented here. Accordingly, it should be noted that the experimentally observed changes in maximum EPR intensity with varying $\bar{\delta}/3\Gamma$ can be much greater than those illustrated in the figures discussed in Sec. III.

III. RESULTS

A. General characteristics of anisotropic spectra

Using the techniques described above, a number of calculations have been made which illustrate the characteristics and spectral features (i.e., angular variations, line shapes, etc.) that have been found to be of the greatest utility in identifying and classifying intermediate Jahn-Teller effects in EPR spectra. In particular, the line shapes for eight values of $\bar{\delta}/3\Gamma$ were calculated for applied magnetic field orientations corresponding to $\vec{H}\|[100]$ and $\vec{H}\|[111]$. Additionally, the angular variations in the $\{100\}$ and $\{110\}$ planes have been calculated for values of $\bar{\delta}/3\Gamma$ identical to those used in the line-shape calculations. Figure 2 shows the calculated line shapes corresponding to the applied magnetic field orientation $\vec{H}\|[100]$ with $\bar{\delta}/3\Gamma = 0.01$, 0.1, 0.2, 0.3, 0.4, 0.5, 1.0, and 5.0. The A_2 level has been assumed to be the lower singlet, and a temperature was assumed such that $kT \ll 3\Gamma$. The calculation was carried out for a microwave frequency of 9.0 GHz, and the effective-Hamiltonian parameters $g_1 = 2.0$ and $qg_2 = 0.05$ were used. The relations given by $r = -\sqrt{2}q$ and $q = \frac{1}{2}$ were employed in accordance with the previously discussed assumptions. As shown in Fig. 2, a value of $\bar{\delta}/3\Gamma = 0.01$ results in a computed line shape which is quite close to that expected for the dynamic Jahn-Teller effect. A slight broadening of the low-field extreme located at $H_2 = h\nu/(g_1 + qg_2)\mu_B$ is already in evidence, however. As $\bar{\delta}/3\Gamma$ increases, this broadening also increases rapidly and is accompanied by a shift of the peak to lower field. The broadening of the low-field peak apparently reaches a maximum between $\bar{\delta}/3\Gamma = 0.3$ and $\bar{\delta}/3\Gamma = 0.5$. Then as the low-field peak sharpens with increasing $\bar{\delta}/3\Gamma$ beyond $\bar{\delta}/3\Gamma = 0.5$, the rate of shift of the peak slows, and the peak reaches a minimum magnetic field position at $H_1 = h\nu/(g_1 + 2qg_2)\mu_B$. The transition has now been made to an almost completely static Jahn-Teller effect with H_1 corresponding to what would ordinarily be called the $g_\parallel$ position for the spectrum, which now has tetragonal symmetry. The position of the high-field peak at $H_3 = h\nu/(g_1 - qg_2)\mu_B$ would also now correspond to the $g_\perp$ position, and the intensity should be twice that of the peak located at the $g_\parallel$ position as is shown in the figure. It should be noted that in this case, (i.e., with coupling to an A_2 level and qg_2 positive) the high-field peak at the magnetic field position H_3 is not shifted as $\bar{\delta}/3\Gamma$ is varied.

In general, the side of the spectrum that is shifted and broadened depends on the sign of qg_2 and on which singlet (i.e., A_1 or A_2) lies lower (see Sec. II C). Once the sign of qg_2 is determined, the lower-lying singlet can be identified using the information summarized in Table I.

In performing EPR experiments on cubic crystals, a technique that is frequently employed is to orient the sample in a manner that permits an effective rotation of the applied magnetic field in a {110} plane. With this type of orientation it is possible to observe the spectral characteristics with the applied field parallel to the cubic principal axes ⟨001⟩, ⟨111⟩, and ⟨110⟩. Accordingly, the dependence on $\bar{\delta}/3\Gamma$ of the position of the peaks in this plane is of interest. Additionally, in analyzing the EPR spectra for intermediate JT cases of the type being treated here, the value of $\bar{\delta}/3\Gamma$ which describes a particular system can be determined by fitting the angular variation of the "shifted side" of the EPR spectrum in a {110} plane. [The effective-Hamiltonian parameters g_1, qg_2, A_1, and qA_2 can first be determined by fitting the unaffected side of the EPR spectrum to Eq.(20).] Figure 3 shows the computed angular variation in the $(1\bar{1}0)$ plane (again excluding any hyperfine structure) for the same $\bar{\delta}/3\Gamma$ values as those employed in calculating the line shapes shown in Fig. 2. For $\bar{\delta}/3\Gamma = 0.01$, the angular variation is seen to be symmetric (to first order) about a constant magnetic field value corresponding to the superimposition of peaks at the orientation $\vec{H}\|[111]$, and the angular variation at values of $\bar{\delta}/3\Gamma < 0.01$ should be accurately described by Eq. (20). As $\bar{\delta}/3\Gamma$ increases in the intermediate region, the angular variation changes in a manner which increases the anisotropy of the "coupled" side of the spectrum until a variation characteristic of three ⟨100⟩ axially symmetric spectra is obtained for $\bar{\delta}/3\Gamma > 5.0$.

The angular variation of the EPR spectrum as

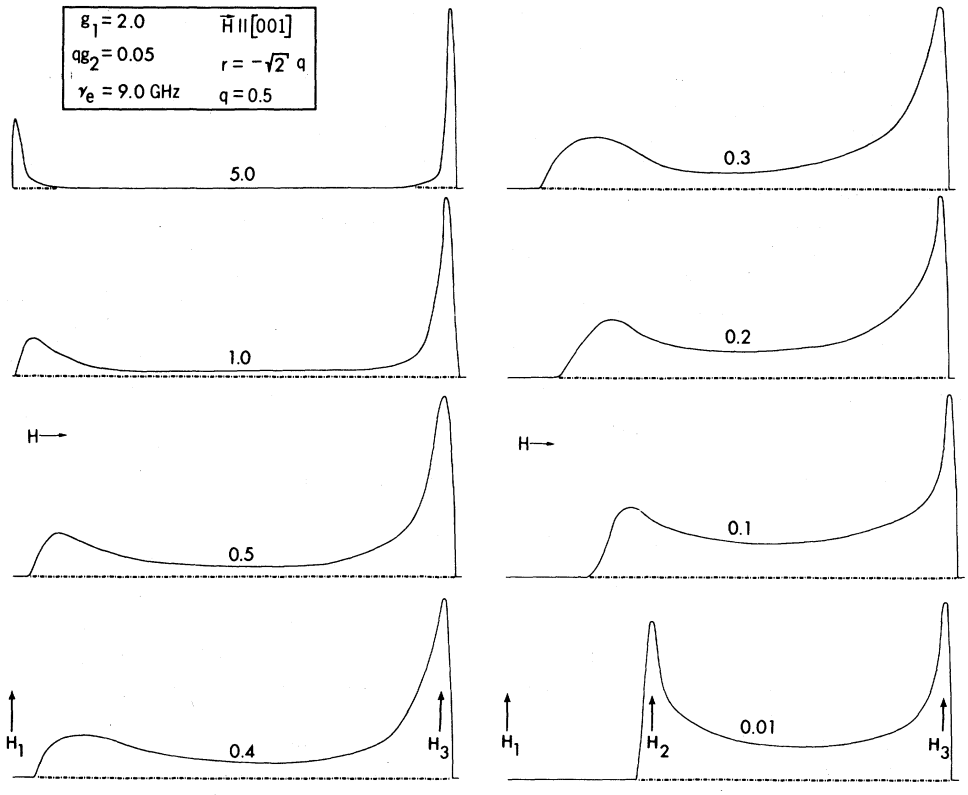

FIG. 2. Dependence of EPR line shapes in the intermediate JT region on the ratio $\bar{\delta}/3\Gamma$ for the magnetic field orientation $\vec{H}\|[001]$. The appropriate value of $\bar{\delta}/3\Gamma$ is placed above the corresponding EPR spectrum. Spectra are calculated assuming that only the lowest strain-split Kramers doublet is populated. Lowest vibronic singlet was assumed to be the A_2 level. Magnetic field values H_1, H_2, and H_3 are given by $H_1 = h\nu/(g_1 + 2qg_2)\mu_B$, $H_2 = h\nu/(g_1 + qg_2)\mu_B$, and $H_3 = h\nu/(g_1 - qg_2)\mu_B$. Intensities of the various spectra have not been normalized relative to each other (after Ref. 6).

the applied magnetic field is rotated in a {100} plane is also of interest. (As a practical consideration, however, the variation in this plane is not as convenient as the {110} plane angular variation for actually determining the values of the effective-Hamiltonian parameters g_1, qg_2, A_1, and qA_2, and the value of $\bar{\delta}/3\Gamma$.) Figure 4 shows the angular variations computed as previously described for the same $\bar{\delta}/3\Gamma$ values used in Figs. 2 and 3. In Fig. 4, the angles 0° and 90° correspond to the $\vec{H}\|[100]$ and $\vec{H}\|[010]$ orientations, respectively, and the angle 45° corresponds to the $\vec{H}\|[110]$ orientation. For the value of $\bar{\delta}/3\Gamma = 0.01$, the calculated angular variation is characteristic of the dynamic Jahn-Teller effect, and the extremes vary as a function of the magnetic field orientation as predicted by Eq. (20). At a value of $\bar{\delta}/3\Gamma = 0.2$, the angular variation in this plane no longer consists of just two components; a weak additional structure (indicated by the dashed line in Fig. 4) appears. As $\bar{\delta}/3\Gamma$ increases beyond the value of 0.2, this structure increases in intensity until at $\bar{\delta}/3\Gamma > 5.0$ it has become part of the angular variation characteristic of three ⟨100⟩ axially symmetric sites.

Although the angular variations shown in Figs. 3 and 4 represent the dependence of the major sharp resonance peaks on the applied magnetic field orientation, the complete line shape in the intermediate JT region exhibits additional structure whose intensity varies depending on the value of $\bar{\delta}/3\Gamma$. For a given general orientation of the applied magnetic field, both the intensities and the magnetic field positions of this structure are observed to change as a function of $\bar{\delta}/3\Gamma$, and the

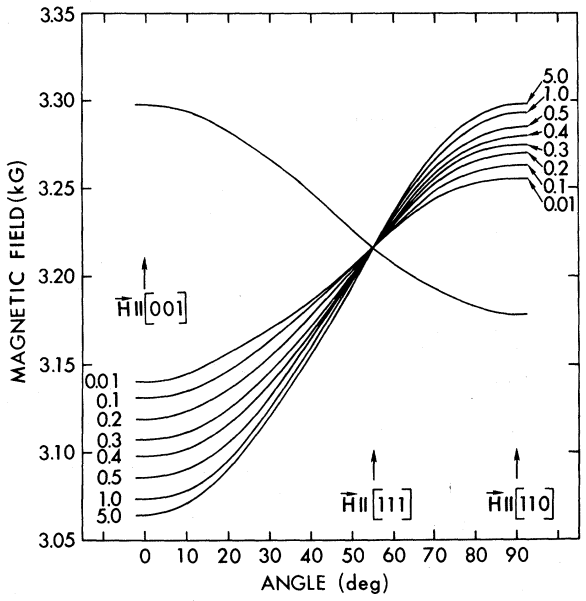

FIG. 3. Angular variation of the peaks of the strain-broadened EPR spectra for applied magnetic field directions in the (110) plane. Appropriate values of $\bar{\delta}/3\Gamma$ are given for each trace. Position of the high-field peak at $\vec{H}\|[100]$ is independent of $\bar{\delta}/3\Gamma$ since qg_2 is positive and the coupling via strain has been assumed to be only to the A_2 excited vibronic singlet. The corresponding angular variation for qg_2 positive with the A_1 singlet lying lower can be obtained approximately by reflecting the curves through the line of constant magnetic field which passes through the superimposition at $\vec{H}\|[111]$ (after Ref. 6).

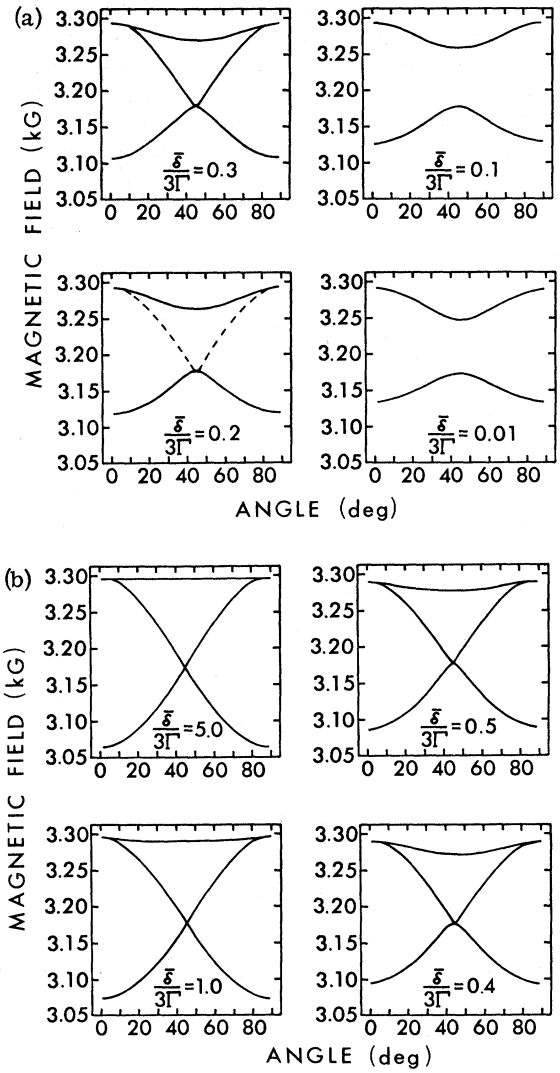

FIG. 4. Angular variation in the (001) plane of the peaks in the EPR spectra for the intermediate JT region. As in Fig. 2 and 3, the following values were used: $\nu = 9$ GHz, $g_1 = 2.0$, $qg_2 = +0.05$. 0°, 45°, and 90° orientations correspond, respectively, to $\vec{H}\|[100]$, $\vec{H}\|[110]$, and $\vec{H}\|[010]$.

components which are weak and broad near one limiting case (i.e., near either the static or dynamic case) will sharpen, increase in intensity, and become the strong components near the opposite limiting case. This effect is best illustrated by a calculation of the variation of the complete spectrum as a function of $\bar{\delta}/3\Gamma$ for an arbitrary general orientation of the applied field (i.e., an orientation that does not correspond to the magnetic field parallel to one of the ⟨001⟩, ⟨111⟩, or ⟨110⟩ axes). Such a calculation is shown in Fig. 5, where the variations of the positions, widths, and intensities of the absorption peaks can clearly be followed in going from one limiting case to the other. The particular magnetic field orientation assumed in Fig. 5 is parallel to a line 30° from the [100] direction and lying in the (001) plane. (It should be noted that for $\bar{\delta}/3\Gamma = 0.0033$ and 0.003, the absorption peak located at the center of the line shape is due to thermal population of the A_2 singlet level. Additionally, the values of $\bar{\delta}/3\Gamma$ employed in these calculated spectra are not identical to those used in the previous figures.) In Fig. 5, the line shape calculated for $\bar{\delta}/3\Gamma = 0.33$ is particularly complex. In an actual resonance experiment, the broad components of the line may not be observed, particularly when synchronous detection techniques are employed and the experimental conditions are optimized to observe the "narrow" absorption peaks.

In addition to the changes observed in the EPR angular variation and general line shape due to changes in $\bar{\delta}/3\Gamma$, a pronounced dependence on $\bar{\delta}/3\Gamma$ is observed for the line shapes observed with $\vec{H} \| \langle 111 \rangle$. In both the dynamic and static limits, the EPR spectrum with $\vec{H} \| \langle 111 \rangle$ of the $^2E \rightarrow A_1$ (or A_2) manifold generally consists (in the absence

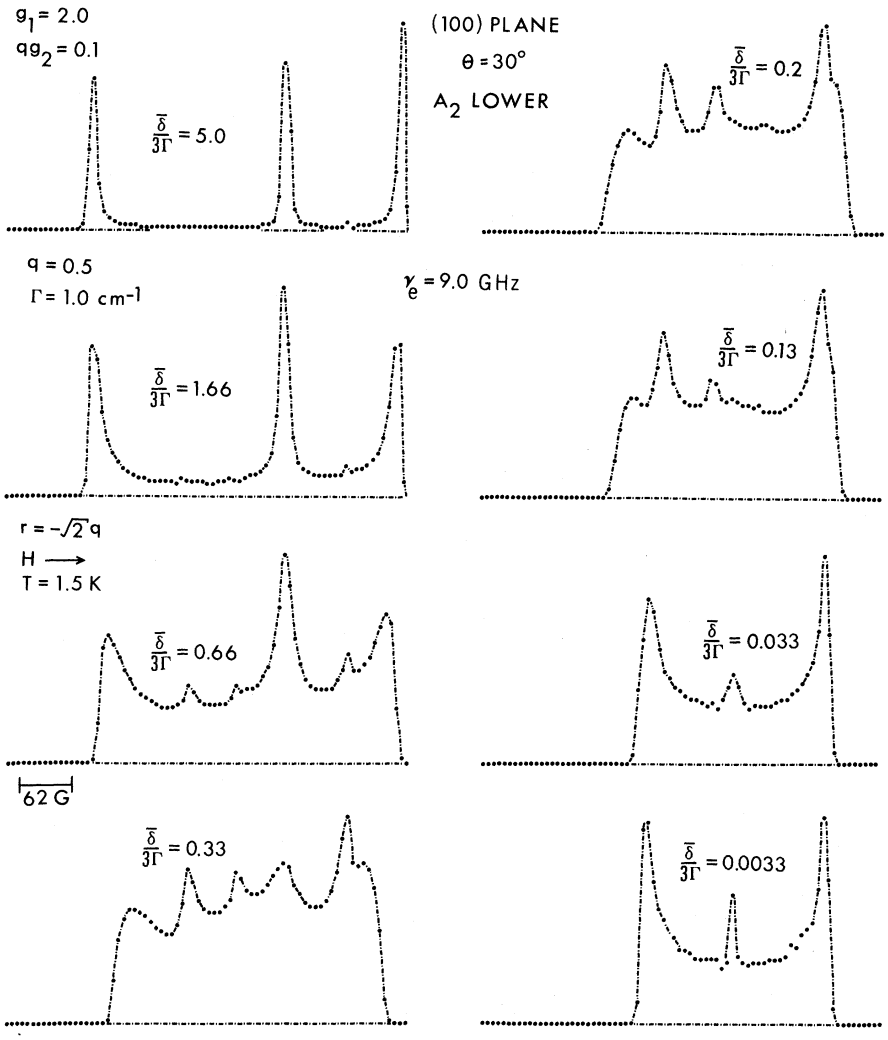

FIG. 5. Dependence of the EPR line shape on $\bar{\delta}/3\Gamma$ for $\vec{H}$ oriented 30° from the [001] direction and lying in the (100) plane. Note that the values of qg_2 and $\bar{\delta}/3\Gamma$ are somewhat different from those used in Figs. 2–4. Changes in intensity, width, and magnetic field position of the "static" and "dynamic" components of the envelope can be clearly followed in going from the dynamic case ($\bar{\delta}/3\Gamma = 0.0033$) to near the static case ($\bar{\delta}/3\Gamma = 5.0$).

of hyperfine structure) of a single symmetric EPR line with a Gaussian or Lorentzian shape. For the dynamic JT effect, the line observed for the orientation $\vec{H}\|\langle 111\rangle$ occurs at a magnetic field corresponding to the g value given by the expression

$$g=[g_1^2+\tfrac{1}{2}(qg_2)^2]^{1/2}, \tag{36}$$

while for the static JT effect the line occurs at the larger g value given by the expression

$$g=[g_1^2+2(qg_2)^2]^{1/2}. \tag{37}$$

This difference in g value is usually small since $g_1 \gg qg_2$. The narrow width of the spectrum observed for $\vec{H}\|\langle 111\rangle$ for the dynamic JT systems results from the fact that with this magnetic field orientation the Zeeman splitting at a particular site is independent of the distribution of random strain between the θ and ϵ compoenents. If appreciable admixture between the ^2E and an excited A_1 or A_2 singlet is present, however, small off-diagonal terms from the anisotropic Zeeman interaction produce a slight dependence of the Zeeman splitting on the value of ϕ. The effect on the EPR spectrum for the ensemble of sites with $\vec{H}\|\langle 111\rangle$ is to distribute the line shape between the magnetic field limits given by Eqs. (36) and (37). Figures 6 and 7 illustrate the effect of the varying ratio of

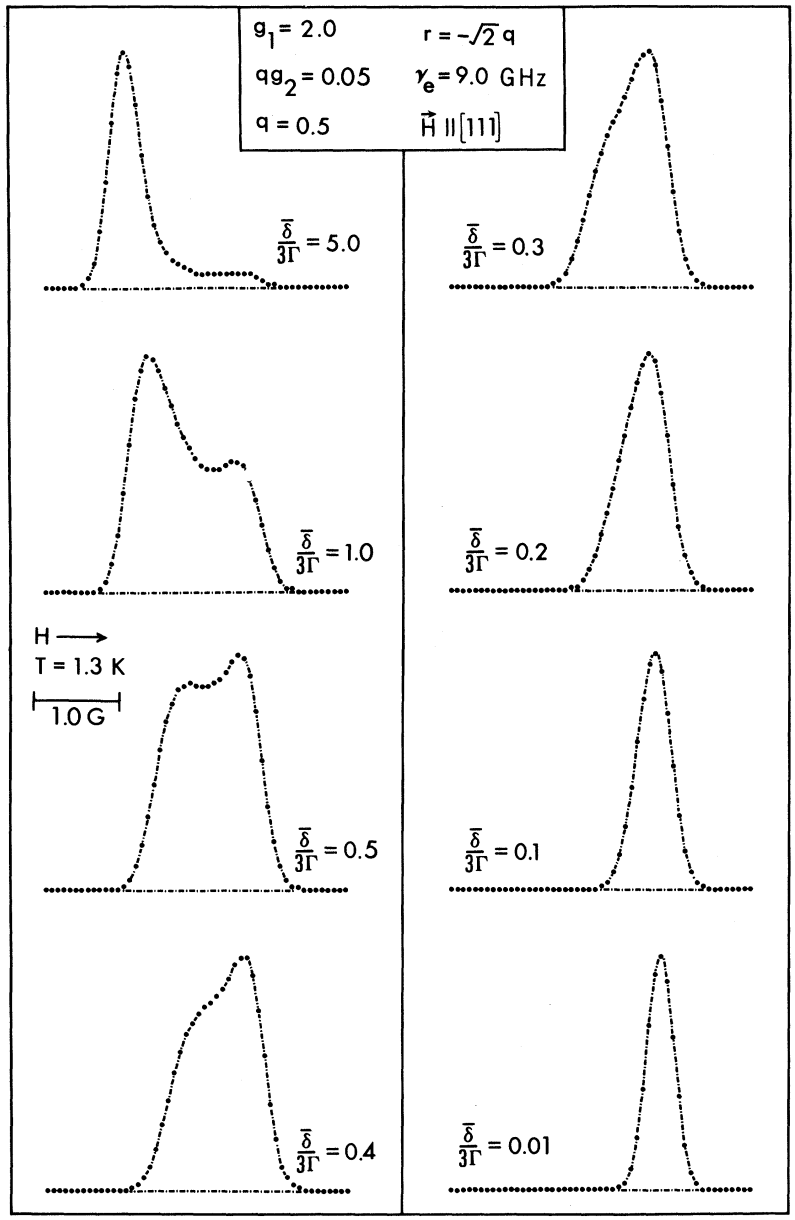

FIG. 6. Dependence of the EPR line shape on $\bar{\delta}/3\Gamma$ for the magnetic field orientation $\vec{H}\|[111]$. $\bar{\delta}/3\Gamma$ values, spin-Hamiltonian parameters, and coupled vibronic singlet state (A_2) are the same as those used for Figs. 2–4. Absorption line shapes given in this figure can be compared with the first derivative spectra given in Fig. 7. It should be noted that intermediate JT effects are still evident in the line shape corresponding to $\bar{\delta}/3\Gamma = 0.5$, and an additional increase in $\bar{\delta}/3\Gamma$ would be necessary in order to obtain the symmetric line shape associated with the "pure static" case.

$\bar{\delta}/3\Gamma$ on the line shapes obtained with $\vec{H}\|\langle 111\rangle$. In Fig. 7, the computed EPR absorption line shapes with $\vec{H}\|\langle 111\rangle$ are displayed for the same $\bar{\delta}/3\Gamma$ values as those used in Figs. 2–4. In Fig. 7, the first derivatives of the absorption spectra shown in Fig. 6 are presented. As $\bar{\delta}/3\Gamma$ is decreased (i.e., with an increasingly dynamic JT effect), the resonance peak at low field decreases in intensity, and the intensity of the high-field peak increases. Approximate equality of the static component of the line shape (at low field) with the dynamic component (high field) occurs at a value of $\bar{\delta}/3\Gamma$ slightly greater than 0.5. The first derivative presentation shown in Fig. 7 is apparently a somewhat more sensitive method of detecting the changes in the line shape due to varying $\bar{\delta}/3\Gamma$ ratios than the absorption spectra shown in Fig. 6. The experimental observation of these asymmetric line shapes

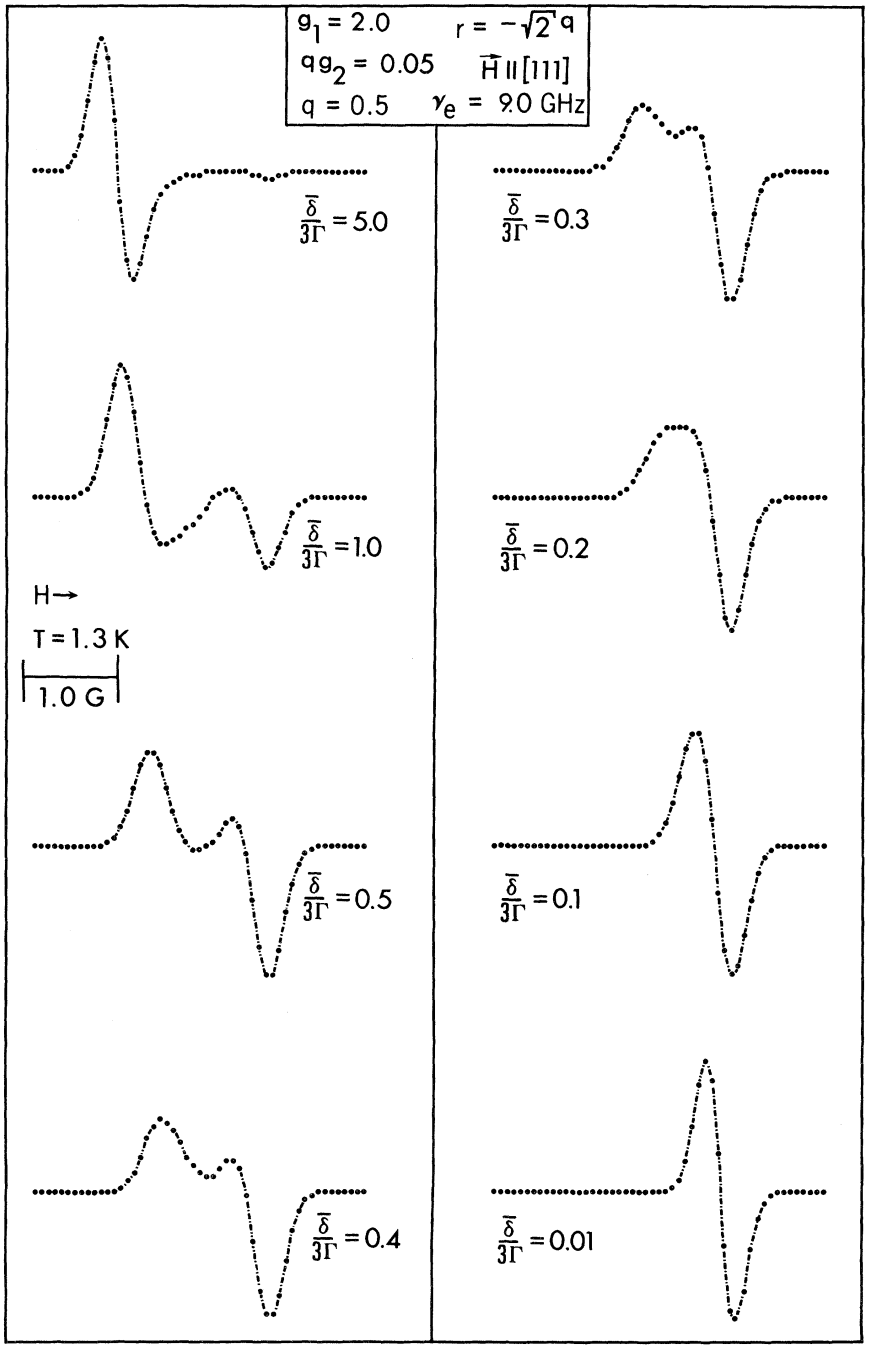

FIG. 7. First derivatives of the EPR absorption spectra given in Fig. 6 are shown. The first derivative is seen to be more sensitive to small changes in line shape for the magnetic field orientation $\vec{H}\|[111]$.

with $\vec{H}\|\langle 111\rangle$ requires relatively narrow line widths. Such line shapes have been observed,[6,7] however, for CaO: Ag^{2+} and CaO: Cu^{2+}.

In Fig. 8, the experimentally observed CaO: Cu^{2+} spectrum obtained at the orientation $\vec{H}\|\langle 111\rangle$ is shown at the top of the figure. The corresponding spectrum computed using the techniques described previously is shown for comparison at the bottom of the figure.[6] A hyperfine splitting appropriate to $I=\frac{3}{2}$ is observed for this system, and the individual line shapes are highly asymmetric. In generating the computed spectrum, the same values of g_1, qg_2, A_1, qA_2, and $\bar{\delta}/3\Gamma$ were used that correctly predicted the angular variation of the CaO: Cu^{2+} EPR spectrum observed as $\vec{H}$ was rotated in the (110) plane. The presence of two Cu isotopes having slightly different nuclear magnetic moments was ignored in the computation. The agreement between the observed and computed EPR spectra is seen to be excellent, with the exception of two small lines (denoted by asterisks in the figure). These lines may be attributed to "forbidden" hyperfine transitions induced by a nuclear quadrupole interaction.[17] This interaction was not included in the generation of the computed spectrum.

As previously noted, random-strain admixture produces a shift in the magnetic field position of the "coupled" side of an essentially dynamic JT spectrum, producing a quasidynamic JT effect. This shift in magnetic field position, however, differs in direction depending upon which of the two Kramers doublets is considered. For $\vec{H}$ in a $\{110\}$ plane, the shift is in such a direction as to increase the anisotropy associated with the lower Kramers doublet resulting from the strain splitting and to decrease the anisotropy of the spectrum associated with the upper strain-split Kramers doublet (see Sec. II C). This effect is illustrated in Fig. 9. The right- and left-hand columns in Fig. 9 correspond respectively to computed EPR spectra for a quasidynamic system in which the magnitude of the random strain was and was not distributed in accordance with Eq. (35). In the undistributed case, as shown on the left-hand side of the figure, δ was set equal to $\bar{\delta}$ throughout the calculation and ϕ was distributed in the range $0 \leq \phi \leq 2\pi$. For both computations, $\bar{\delta}/3\Gamma$ was set equal to 0.13 and $\vec{H}$ was oriented in the [100] direction. The spectra at the top of each column of Fig. 9 are due only to the upper strain-split Kramers doublet resulting from the ^2E level, while the spectra in the center of each column result only from the lower strain-

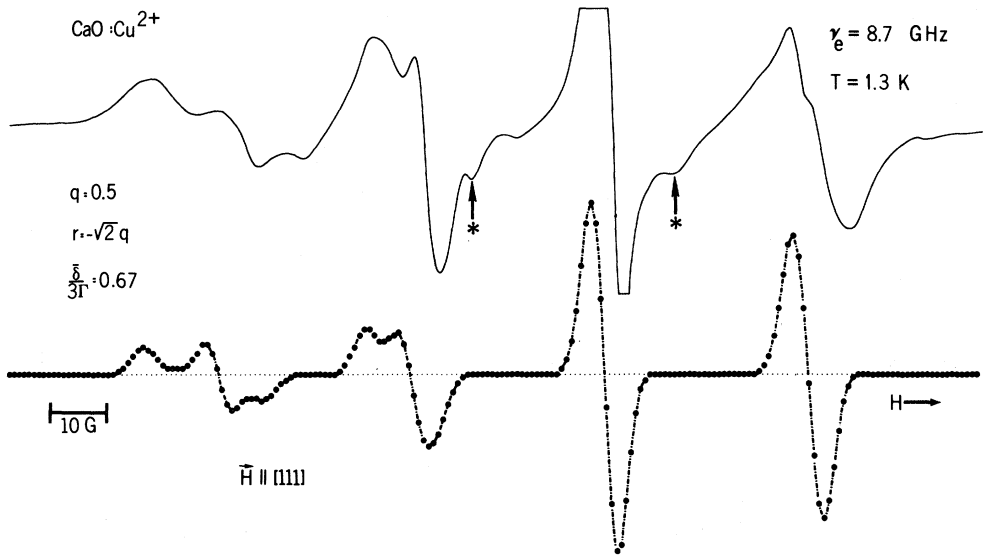

FIG. 8. (Top) Experimentally determined first-derivative EPR spectrum for Cu^{2+} in CaO observed with $\vec{H}\|[111]$. Extremities of the largest hyperfine "line" are clipped due to the high amplifier gain used in order to illustrate the broader, less intense structure. (Bottom) EPR spectrum calculated for CaO:Cu^{2+} using the effective-Hamiltonian parameters and the $\bar{\delta}/3\Gamma$ value which were determined from the angular variation observed in the (110) plane. Two features indicated by asterisks in the upper trace are believed to be "forbidden" transitions induced by the nuclear quadrupole interaction. Effects of the nuclear quadrupole interaction were not included in the calculation (after Ref. 6).

split Kramers doublet. The spectra shown at the bottom of each column represent the result of summing the spectra due to both Kramers doublets. Since A_2 was assumed to be the lower singlet and qg_2 is positive, the low-field side of the spectrum is "coupled" by the random strain. The lower-energy Kramers doublet has its low-field peak shifted to lower field, while the corresponding peak of the upper Kramers doublet is shifted to higher field. The actual experimental observation of two such peaks on one side of the spectrum for a quasidynamic JT system would depend on the thermal population of the upper state. In the case where the strain is distributed in magnitude, the low-field peak of the upper Kramers doublet is shifted back on itself in a manner which distorts the shape of the peak. Due to the distribution of strain magnitude, it would probably be difficult to distinguish the contribution of the upper Kramers doublet in a quasidynamic case even at elevated temperatures.

Figure 10 illustrates the effect on the EPR line shape when the tunneling splitting 3Γ is varied while $\bar{\delta}/3\Gamma$ is held constant. In Fig. 10, $\bar{\delta}/3\Gamma$, g_1, and qg_2 have the same values as those shown in Fig. 9. The magnetic field orientation corresponds to $\vec{H}\|[100]$, and Γ is varied from 0.1 to 5.0 cm^{-1}. The effect of this variation in Γ is to change the relative population of the three Kramers doublets. For $\Gamma = 5.0$ cm^{-1}, the EPR spectrum consists mainly of the contribution due to the ground Kramers doublet and is almost identical in shape to the spectrum shown at the right center of Fig. 9. As Γ is decreased to 2.0 cm^{-1}, the relatively large contribution from the first excited Kramers doublet is observed in the appearance of the sharp peak which is about 100 G higher in field than that of the low-field peak (see Fig. 10). Additional decreases in Γ produce appreciable population of the second excited Kramers doublet and result in the appearance of a peak near the center of the spectrum. In the spectra shown in Fig. 10, the admixture of the ^2E level into the A_2 level produces an appreciable broadening of the peak associated

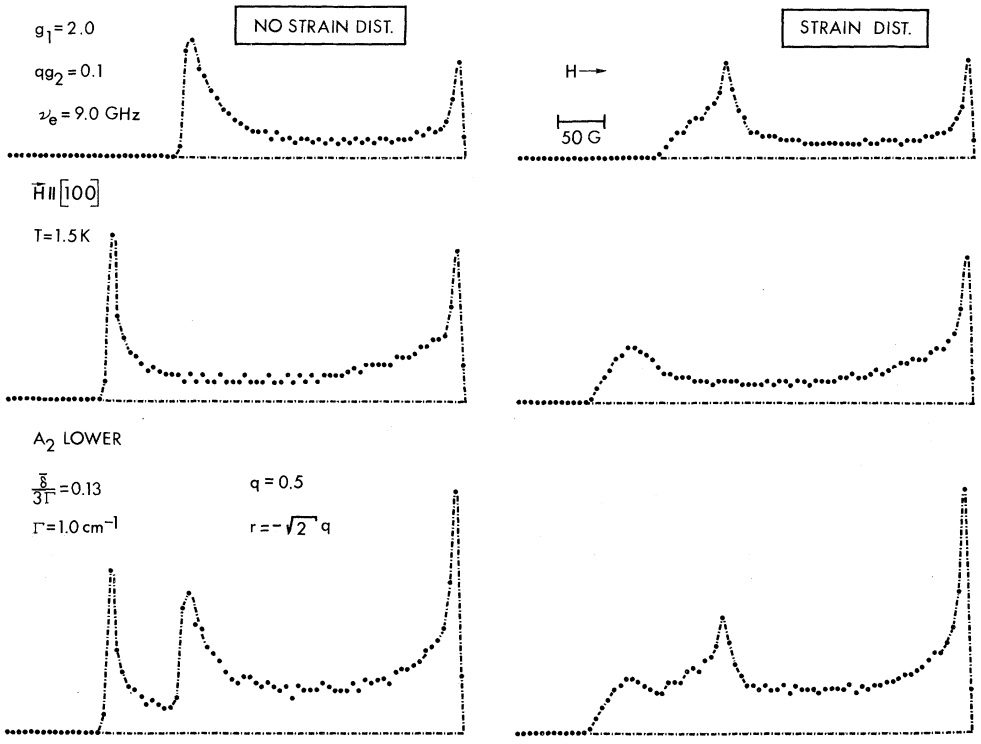

FIG. 9. Left-hand side: EPR spectra corresponding to the first excited (top) and ground (center) Kramers doublet which result from a ^2E vibronic ground state with weak random-strain coupling to a A_2 level. Magnitude of the random-strain splitting was assumed constant from site to site in the crystal. Top and center spectra are summed in the bottom trace. Right-hand side: EPR spectra corresponding to those at the left-hand side of the figure are shown, but now the random-strain magnitude has been distributed from one site in the crystal to another in accordance with Eq. (35).

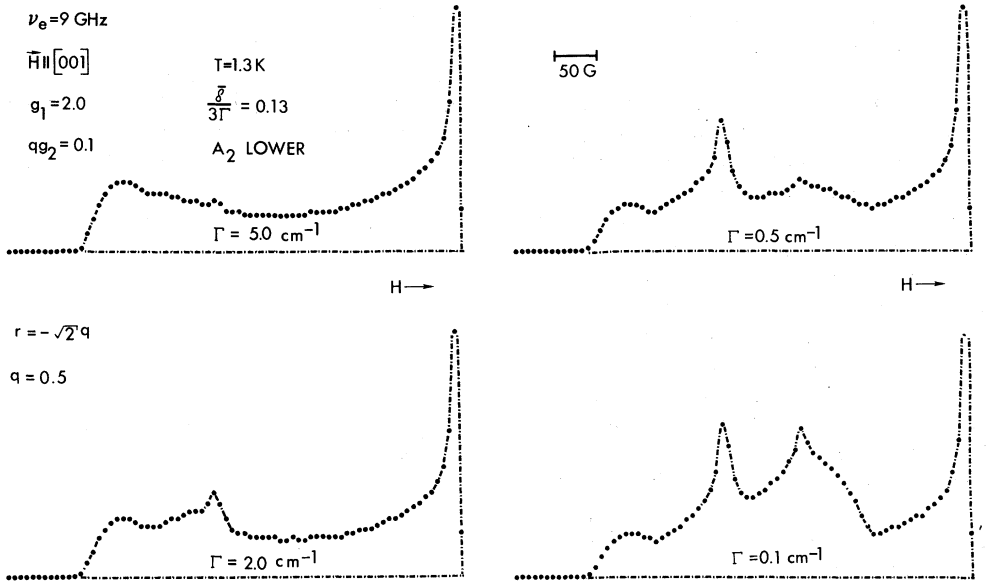

FIG. 10. Dependence on the value of Γ for the EPR line shape resulting from weak random-strain coupling of the ^2E and A_2 states. Value of $\bar{\delta}/3\Gamma$ is fixed at 0.13 for each trace. Relative contributions of the excited Kramers doublets to the absorption intensity increase as Γ decreases in value.

with the A_2 state. It should be noted also that the variation demonstrated in Fig. 10 is equivalent to a variation in kT.

B. Origin of isotropic EPR spectrum for ^2E vibronic states in dynamic and intermediate JT regions

For those systems in which the JT effect can be classified as either pure dynamic or quasidynamic according to the definitions discussed previously, the observed low-temperature EPR spectra have consisted of both isotropic and anisotropic components. The isotropic component of the spectra corresponding to this region of $\bar{\delta}/3\Gamma$ values can result from averaging by relaxation of varying portions of the strain-broadened anisotropic spectrum, from thermal population of the first excited vibronic singlet, or from a combination of these effects. The assignment of the origin of these isotropic spectra has received a considerable amount of attention in previous work on systems in the pure dynamic and quasidynamic regions. Several criteria have been proposed for the purpose of distinguishing between the two possibilities. The results of our present calculations of line shapes reveal some interesting features which strongly affect the validity of some of the previously proposed criteria for distinguishing the origin of the isotropic spectra.

As noted earlier, for the pure dynamic JT effect the observed resonance line shape as shown in Fig. 11 (top) is an envelope of transitions which are symmetrically distributed (in first order) about a central magnetic field value which corresponds to the position of the resonance line at the orientation $\vec{H}||\langle 111\rangle$. As pointed out by Ham,[13] phonons can produce transitions of the type indi-

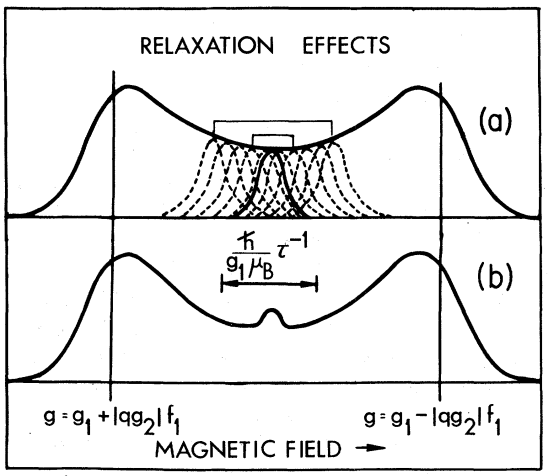

FIG. 11. Effect on a "purely dynamic" EPR spectrum of vibronic relaxation between strain-split levels. Rapid vibronic relaxation can produce an essentially isotropic peak at the central field position. Portion of the strain-broadened line which satisfies the condition for averaging by relaxation will vary with the orientation of the applied magnetic field (after Ref. 2).

cated by the curved arrows shown in Fig. 1 to motionally average a portion of the anisotropic spectrum. This averaging by relaxation results in an isotropic spectrum at the approximate center of the strain-broadened line, as illustrated in Fig. 11 (bottom). In previous investigations of the dynamic JT effect in which the origin of the observed isotropic spectrum was ascribed to such averaging by relaxation, some of the criteria which formed the basis for this assignment were as follows: For La^{2+} in $SrCl_2$ and a number of other systems characteristic of the dynamic Jahn-Teller effect, changes were observed in the apparent intensity and the linewidth of the isotropic spectrum as a function of the orientation of the applied magnetic field.[2,5] (Here the term "apparent intensity" refers to the peak-to-peak amplitude of the first derivative of absorption.) The observed isotropic spectrum increased in apparent intensity and narrowed as the applied field approached the orientation $\vec{H}\|\langle 111\rangle$, and this behavior was said to exclude the possibility that the origin of the isotropic spectrum was due to population of the first excited vibronic singlet. The argument which formed the basis for this criterion was based on the idea that the portion of the strain-broadened line which satisfied the condition for averaging by relaxation would increase as the applied magnetic field approached the orientation $\vec{H}\|\langle 111\rangle$ (i.e., the number of transitions within $\frac{1}{2}\Delta\nu$ of the center of the envelope of transitions would increase as $\vec{H}$ neared the $\langle 111\rangle$ orientation so that more transitions would satisfy the condition for averaging by relaxation given by the expression $\tau^{-1} \gg 2\pi\Delta\nu$, where τ^{-1} is the relaxation rate).[2]

In order to determine the corresponding characteristics of the isotropic spectrum when it is due solely to thermal population of the first excited vibronic singlet, a calculation of the complete (i.e., anisotropic and isotropic) spectrum for a quasidynamic case was performed. The results of this calculation are illustrated in Fig. 12. A value of $\bar{\delta}/3\Gamma = 0.033$ was chosen in carrying out this calculation because it was estimated that this is approximately the largest value that $\bar{\delta}/3\Gamma$ could assume without producing perceptible changes in the angular variation characteristic of the dynamic JT effect. (This estimate was based on known linewidths for such systems and on our experience relating to the experimental accuracy obtainable in the measurement of line positions.) The isotropic line located at the center of the computed spectra shown in Fig. 12 clearly narrows and increases in intensity as the applied magnetic field approaches the [111] direction which, in this case, corresponds to the angle $\theta = 55°$. This behavior is identical to that expected for isotropic lines which are produced by averaging by relaxation. Accordingly, the observation of such behavior does not, in itself, serve to distinguish between the possible origins of the isotropic spectrum. Figure 13 illustrates the results of a calculation which is somewhat similar to that shown in Fig. 12, except that the values $q = -r = 0.5$ have been used instead of the values $q = 0.5$ and $r = -\sqrt{2}q$. The relation $q = -r$

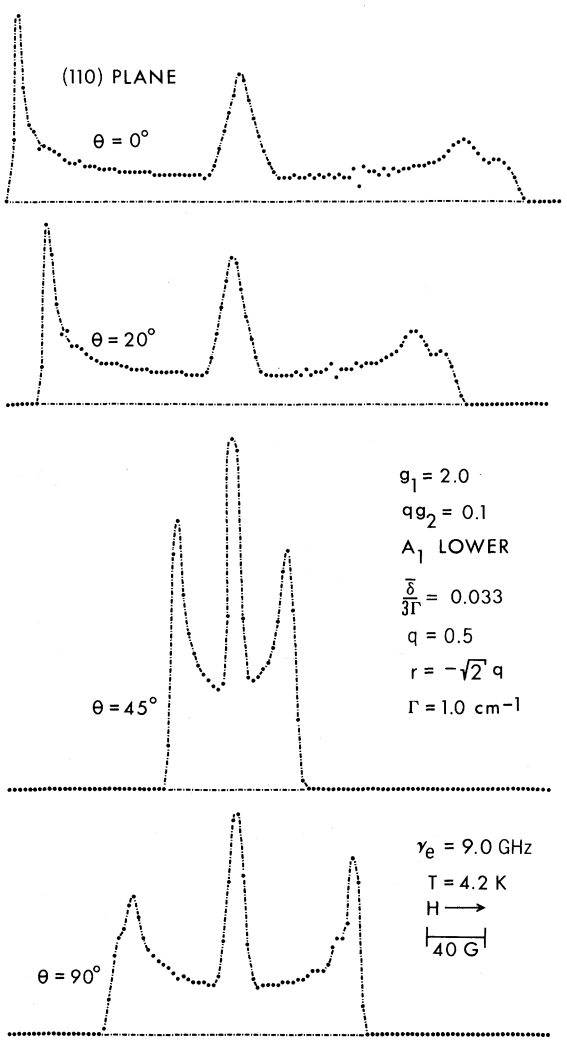

FIG. 12. Angular variation in the (110) plane of the EPR line shape with $\bar{\delta}/3\Gamma = 0.033$. Angle $\theta = 0°$ corresponds to $\vec{H}\|[001]$. Line width and intensity variation of the center peak is due solely to population of the excited vibronic singlet. The structure consisting of the two peaks which are visible at the high-field extreme of the line shape for $\theta = 0°$ and $\theta = 20°$ (and which are slightly resolved for $\theta = 90°$) arises as a result of thermal population of both Kramers doublets. Effect is discussed in detail in Sec. II C of the text and is illustrated in Fig. 9.

$=0.5$ is appropriate to strong JT coupling with weak warping terms. Similar but less severe narrowing and intensity changes in the isotropic spectrum are present under these conditions, and effects more like those shown in Fig. 12 are obtained only by using increased values for $\bar{\delta}/3\Gamma$.

An additional criterion previously used to distinguish between the possible origins of the isotropic spectrum was based on the observation of increased intensity of the isotropic lines as a function of sample treatment, which corresponded to increasing the strain present in the sample.[5] Ham has previously shown[1] that the relaxation rate for the direct process increases quadratically with increasing δ, and therefore an increase in the intensity of the isotropic spectrum with increasing strain is predicted.

The effects of increasing strain on the isotropic spectrum due only to population of the excited vibronic singlet are illustrated in Fig. 14. The complete anisotropic and isotropic spectrum has been calculated for four different values of $\bar{\delta}/3\Gamma$, with 3Γ held constant at 3.0 cm^{-1}. With increasing $\bar{\delta}/3\Gamma$, which in this case corresponds to increasing $\bar{\delta}$, the isotropic line is observed to broaden and decrease in intensity; this behavior is opposite to that expected for a system in which the isotropic spectrum arises as a result of averaging. This result, however, should be viewed with caution; it does not necessarily establish the criterion of increasing strain versus increasing intensity as a means of identifying the process of averaging by relaxation. The reason for this uncertainty lies in the fact that while it is quite easy in a calculation of the type performed here to hold 3Γ constant, in an actual system, changes which are sufficiently severe to affect the gross properties of the host crystal will undoubtedly change the value of 3Γ. What the nature of such changes would be, or if they might serve to counteract the effects shown in Fig. 14 and due to increases in $\bar{\delta}$, has not been determined at this time. In this regard, it should be noted that for Rh^{2+} in MgO (which appears to be a quasistatic JT system) Suss *et al.*[18] reported that reduction in a hydrogen atmosphere produced a decrease in the intensity of the isotropic lines. This type of behavior is, of course, exactly opposite to that observed by Herrington, Estle, and Boatner[5] for La^{2+} in $SrCl_2$. The dependence of the characteristics of the isotropic spectrum on sample preparation currently represents an open area of inquiry.

An additional investigation that would be of interest in terms of the present topic is the calculation of possible anisotropy in the positions of the "iso-

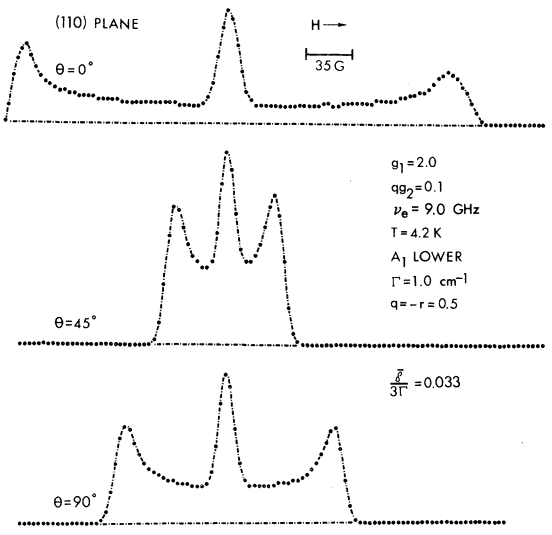

FIG. 13. Angular variation similar to that given in Fig. 12, but for $q=-r=0.5$. Relation between q and r is appropriate to strong JT coupling with weak warping terms. Variation in the line shape of the center peak is much less than that shown in Fig. 12.

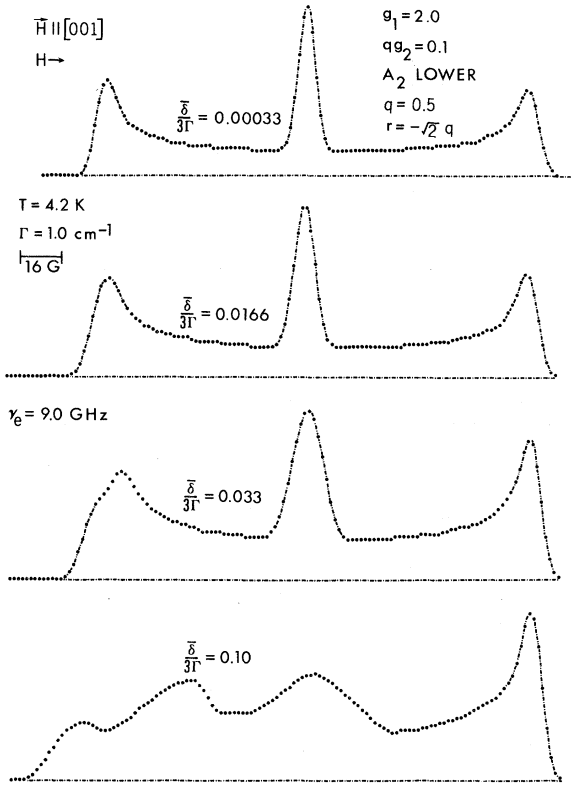

FIG. 14. Dependence on $\bar{\delta}/3\Gamma$ of the line width of the isotropic peak. Given $\bar{\delta}/3\Gamma$ values are all appropriate to a relatively dynamic JT effect.

tropic" lines for systems which exhibit fairly large hyperfine splittings. Coupling via strain and the Zeeman interaction between the ground ^2E level and the vibronic singlet level should result in an anisotropy in the spectrum due to population of the vibronic singlet; it would be useful to determine if the anisotropy was similar to that reported previously for systems characteristic of the pure dynamic case.[3] In the absence of an experiment employing uniaxial stress, perhaps one of the strongest tests of the origin of the isotropic spectrum would result simply from an observation of the absence of any effects on the anisotropic spectrum which are characteristic of the quasidynamic JT effect. If such effects are not observed, the singlet is probably sufficiently removed in energy from the ground state to preclude significant population of this state at liquid-helium temperatures.

IV. SUMMARY

In the present work, the EPR line shapes and angular variations associated with random-strain-coupled ^2E and A_1 (or A_2) vibronic states have been calculated for varying ratios of random-strain splitting to tunneling splitting ($\overline{\delta}/3\Gamma$). In particular, for $\overline{\delta}/3\Gamma$ values in the region of intermediate JT effects, the EPR line shapes and angular variations have been calculated for magnetic field orientations in the {100} and {110} planes. Intermediate JT effects in the EPR line shapes for $\vec{H}\|[111]$ have also been calculated in detail. The evolution of the spectral features resulting from these calculations has been discussed as the value of $\overline{\delta}/3\Gamma$ is varied between the dynamic and static limits. The spectral features which are characteristic of intermediate JT effects have been described and compared with corresponding features associated with the static and dynamic JT effects and with previously reported EPR spectra.

Additionally, for systems exhibiting a quasidynamic JT effect, the EPR spectra have been examined for each of the three Kramers doublets resulting from the slightly admixed ^2E and A_1 (or A_2) manifold. The dependence on $\overline{\delta}/3\Gamma$ and magnetic field orientation has been calculated in particular detail for the relatively isotropic EPR spectrum resulting from the most energetic Kramers doublet (having predominately A_1 or A_2 character). The calculated linewidth variation of this spectrum tends to invalidate a previously used criterion for distinguishing the origin of the isotropic EPR line observed for dynamic JT systems. The implications of these calculations have also been discussed as they relate to another test for the assignment of the isotropic EPR spectrum observed for the dynamic JT effect.

V. ACKNOWLEDGMENTS

The authors are indebted to L. L. Chase for information that was very valuable in the early phases of this investigation. Additionally, the encouragement of F. S. Ham and the comments of M. M. Abraham on the manuscript are appreciated.

[1]F. S. Ham, in *Electron Paramagnetic Resonance*, edited by S. Geschwind (Plenum, New York, 1972), and references therein.
[2]J. R. Herrington, T. L. Estle, L. A. Boatner, and B. Dischler, Phys. Rev. Lett. 24, 984 (1970).
[3]J. R. Herrington, L. A. Boatner, T. J. Aton, and T. L. Estle, Phys. Rev. B 10, 833 (1974).
[4]J. R. Herrington, T. L. Estle, and L. A. Boatner, Phys. Rev. B 7, 3003 (1973).
[5]J. R. Herrington, T. L. Estle, and L. A. Boatner, Phys. Rev. B 3, 2933 (1971).
[6]R. W. Reynolds, L. A. Boatner, M. M. Abraham, and Y. Chen, Phys. Rev. B 10, 3802 (1974).
[7]L. A. Boatner, R. W. Reynolds, M. M. Abraham, and Y. Chen. Phys. Rev. Lett. 31, 7 (1973).
[8]A. Schoenberg, J. T. Suss, Z. Luz, and W. Low, Phys. Rev. B 9, 2047 (1974).
[9]L. A. Boatner, R. W. Reynolds, M. M. Abraham, and Y. Chen, Bull. Am. Phys. Soc. 18, 448 (1973).
[10]R. W. Reynolds, L. A. Boatner, M. M. Abraham, and Y. Chen, Bull. Am. Phys. Soc. 19, 326 (1974).
[11]R. W. Reynolds, L. A. Boatner, M. M. Abraham, and Y. Chen, Bull. Am. Phys. Soc. 18, 448 (1973).
[12]L. L. Chase, Phys. Rev. B 2, 2308 (1974); Phys. Rev. Lett. 23, 275 (1969).
[13]F. S. Ham, Phys. Rev. 166, 307 (1968). See also, G. D. Watkins and F. S. Ham, Phys. Rev. B 1, 4071 (1970).
[14]A preliminary account of this work was presented in L. A. Boatner and R. W. Reynolds, Bull. Am. Phys. Soc. 19, 326 (1974).
[15]W. Moffitt and W. Thorson, Phys. Rev. 108, 1251 (1957); H. C. Longuet-Higgens, U. Öpik, M. H. L. Pryce, and R. A. Sack, Proc. R. Soc. Lond. A 244, 1 (1958).
[16]F. I. B. Williams, D. C. Krupka, and D. P. Breen, Phys. Rev. 179, 225 (1969).
[17]J. R. Herrington, T. L. Estle, and L. A. Boatner, Phys. Rev. B 5, 2500 (1972).
[18]J. T. Suss, A. Raizman, S. Szapiro, and W. Low, J. Magn. Reson. 6, 438 (1972).